Coordinated phenotype switching with large-scale chromosome flip-flop inversion observed in bacteria

Longzhu Cui[1,2], Hui-min Neoh[3], Akira Iwamoto, and Keiichi Hiramatsu

Department of Bacteriology, Faculty of Medicine, Juntendo University, 2-1-1 Bunkyo-Ku, Tokyo, Japan

AUTHOR SUMMARY

The genome inversion, a reversal of a large segment of a chromosome, is thought to play an important role in maintaining cell subpopulations, contributing various biological features in bacteria, and permitting adaptation to changes in the physical environment. Although the evidence for recurrent genome inversion is widely observed in nature when the genomes of closely related species are compared (1, 2), little is known about the mechanism of occurrence and the physiological effect of recurrent genome inversion. In this study, we clarified that the *Staphylococcus aureus* clinical strain Mu50Ω undergoes frequent, large-scale genome reversible inversion during in vitro cultivation.

The strain Mu50Ω was isolated from a patient with a relapsed surgical site infection. When streaked onto agar plates, this strain consistently formed colonies of two distinct sizes, despite repeated colony purification (Fig. P1*A*). One of the subpopulations had a slow-growing phenotype, and was therefore designated as the small colony variant (SCV). Such a phenotype of *S. aureus* has been previously associated with infection persistence and relapse (3). The other subpopulation retained normal growth capability, therefore forming colonies of normal size. This subpopulation was therefore designated as the normal colony variant (NCV) in this study. We further found that these two distinct cell subpopulations could repeatedly transition from one to the other. Additional investigation revealed that colonies of both types were persistently observed in the descendants of both types of originating cell populations, although the ratios of NCV to SCV varied. The prevalence of NCV in the SCV-descendant cell populations was ~0.1–0.3%, compared with 90–99% in the NCV-descendant cell populations.

To understand the mechanism of phenotypic switching, we picked one colony from each subpopulation to establish the Mu50Ω1 (SCV) and Mu50Ω2 (NCV) strains (Fig. P1*A*) and conducted comparative phenotypic and genetic studies, including whole-genome sequence comparison. The phenotype of a mixed colony persisted because of the two-way transition between NCV and SCV during the growing process. The SCV colonies were distinguishable by various characteristics.

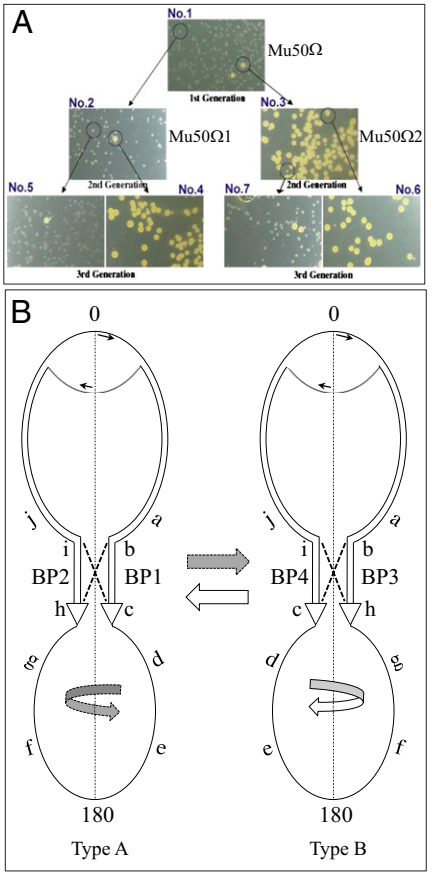

Fig. P1. Characteristics of *S. aureus* Mu50Ω and its derivatives. (*A*) Cell populations of Mu50Ω consist of two subpopulations of cells that produce small- and normal-sized colonies, respectively, on agar plates. Small colony descendants (SCV or Mu50Ω1) mainly form small colonies with a minor proportion of normal colonies (*A*; Nos. 2, 5, and 7), whereas normal colony descendants (NCV or Mu50Ω2) mainly form normal colonies with a small proportion of small colonies (*A*; Nos. 3, 4, and 6), thus reflecting colony-phenotype conversion. (*B*) Genomic comparisons indicate that approximately half of the chromosome genome of SCV is inverted relative to that of NCV. An additional study reveals that the phenotype conversion between NCV and SCV is mediated by reversible genome inversion through two mutually homologous loci present in the left and right chromosome replichores (i.e., genome halves that replicate). BP, breakpoint. Letters a–j indicate nucleotide sequence order along the genome.

In addition to smaller colony size, SCV exhibited less colony pigmentation, impaired hemolytic activity on blood agar, and susceptibility to certain types of antibiotics. Whole-genome sequencing revealed that Mu50Ω2 has a circular chromosome, almost half of which inverts in orientation relative to that of the alternative Mu50Ω1 genome (Fig. P1*B*). This inversion was reversible, which results in the phenotypic switching of the two bacterial subpopulations.

It remained unclear, however, how SCV was able to persist in the culture despite its low growth rate relative to NCV. To answer this question, we developed a mathematical model based on the standard Lotka–Volterra equation for the competitive growth of two cell subpopulations, with some modifications made by incorporating the flip-flop chromosome inversion mechanism and bacterial degradation effects. To reproduce the experimental growth curve data, a difference in the rates of chromosome inversion in SCV and NCV will be necessary, with a rate ~12.5-fold greater in SCV cells compared with NCV cells. When this condition is satisfied, cultures of either SCV or NCV could constantly maintain the two subpopulations.

Transcriptional profiling revealed that the expression of dozens of genes involved in energy metabolism is downregulated in Mu50Ω1, or SCV, compared with Mu50Ω2, or NCV. This may be associated with the SCV phenotype, but

Author contributions: L.C. and K.H. designed research; L.C. and H.-m.N. performed research; L.C. and A.I. analyzed data; and L.C., H.-m.N., A.I., and K.H. wrote the paper.

The authors declare no conflict of interest.

This article is a PNAS Direct Submission.

Freely available online through the PNAS open access option.

[1]To whom correspondence should be addressed. E-mail: longzhu@insti.kitasato-u.ac.jp.

[2]Present address: Research Center for Antiinfectious Drugs, Kitasato Institute for Life Science, Kitasato University, 5-9-1 Shirokane, Minato-ku, Tokyo 108-8641, Japan.

[3]Present address: UKM Medical Molecular Biology Institute, Universiti Kebangsaan Malaysia, 56000 Cheras, Kuala Lumpur, Malaysia.

See full research article on page E1647 of www.pnas.org.

Cite this Author Summary as: PNAS 10.1073/pnas.1204307109.

the reason why genome inversion could lead to such a change in the transcriptional profile remains unknown. The chromosome recombination sites involved in the inversion were identified to be the two mutually homologous loci present in the left and right chromosome replichores, the two segments of the bacteria's genome that are oppositely replicated during cell division (Fig. P1*B*). Homologous recompilation mediated by the DNA-repair enzyme RecA is considered to be involved in the inversion and asymmetry inversion rates between SCV and NCV.

The biological and medical implications for the chromosome inversion in Mu50Ω remain to be elucidated. However, our study has revealed that large-scale, reversible chromosome inversion could be one of the ingenious strategies that *S. aureus* uses to survive in adverse environments. The SCVs facilitate escape from immune attacks, whereas the NCVs are resistant to antibiotic treatment during infection.

1. Ford EB (1965) *Genetic Polymorphism* (Faber and Faber, London).
2. Darling AE, Miklós I, Ragan MA (2008) Dynamics of genome rearrangement in bacterial populations. *PLoS Genet* 4:e1000128.
3. Proctor RA, et al. (2006) Small colony variants: A pathogenic form of bacteria that facilitates persistent and recurrent infections. *Nat Rev Microbiol* 4:295–305.

Coordinated phenotype switching with large-scale chromosome flip-flop inversion observed in bacteria

Longzhu Cui[1,2], Hui-min Neoh[3], Akira Iwamoto, and Keiichi Hiramatsu

Department of Bacteriology, Faculty of Medicine, Juntendo University, 2-1-1 Bunkyo-Ku, Tokyo, Japan

Edited by Richard P. Novick, New York University School of Medicine, New York, NY, and approved December 1, 2011 (received for review March 16, 2012)

Genome inversions are ubiquitous in organisms ranging from prokaryotes to eukaryotes. Typical examples can be identified by comparing the genomes of two or more closely related organisms, where genome inversion footprints are clearly visible. Although the evolutionary implications of this phenomenon are huge, little is known about the function and biological meaning of this process. Here, we report our findings on a bacterium that generates a reversible, large-scale inversion of its chromosome (about half of its total genome) at high frequencies of up to once every four generations. This inversion switches on or off bacterial phenotypes, including colony morphology, antibiotic susceptibility, hemolytic activity, and expression of dozens of genes. Quantitative measurements and mathematical analyses indicate that this reversible switching is stochastic but self-organized so as to maintain two forms of stable cell populations (i.e., small colony variant, normal colony variant) as a bet-hedging strategy. Thus, this heritable and reversible genome fluctuation seems to govern the bacterial life cycle; it has a profound impact on the course and outcomes of bacterial infections.

genome rearrangement | heterogeneity of bacterial population | phase variation

Bacterial growth is usually considered to be the result of a cell division that yields genetically identical siblings. However, it has long been recognized that within the isogenic populations, bacterial cells can display various phenotypes as a result of regulatory diversification benefiting both cell survival and growth (1, 2). This population diversity or cell individuality, most readily visible as colony variation, is relevant to cellular differentiation associated with bacterial virulence and facilitates population survival amid changing environmental conditions (3, 4) (e.g., evading adaptive immune responses), which has profound implications for treatment of infections (1, 5).

The bacterial small colony variant (SCV) was initially described a century ago as a slow-growing aberrant form of WT bacteria. Since then, being implicated in persistent, relapsing, and antibiotic-resistant infections, SCV has been described for a wide range of bacterial genera and species, including *Staphylococcus*, *Pseudomonas*, *Burkholderia*, *Salmonella*, *Vibrio*, *Shigella*, *Brucella*, *Escherichia*, *Lactobacillus*, *Serratia*, and *Neisseria* species (6). Although there are many studies addressing the mechanism of SCV occurrence, where the findings include electron transport deficiencies or menadione, hemin, or thymidine auxotrophicity attributable to the mutations in genes associated with the bacterial metabolic pathway, there are no data available about the genetic events responsible for the reappearance of a rapidly growing form (WT), namely, the normal colony variant (NCV), and the frequently reversible reversion between SCV and NCV (6–10).

We present here a study on the *Staphylococcus aureus* strain that simultaneously produces two distinct colony variations, NCV and SCV. We found that the two variants constantly flipped between each other with unequal frequencies, but this variation was self-organized so as to maintain blended cell progenies with two distinct ratios of SCV/NCV in either variant. The bidirectional reversion of the two variants was driven by a reversible large-scale chromosome inversion (referred to as a flip-flop inversion). The coexistence of these two variants appears to be a bet-hedging strategy for coping with uncertain environments.

Results and Discussion

Bidirectional High-Frequent Conversion Between SCV and NCV. *S. aureus* Mu50Ω is a clinical strain isolated from a patient who was repeatedly hospitalized because of relapsed surgical site infections that persisted for 3.5 y (11). This strain was characterized as SCV (Fig. 1*A*) because it grew slowly on routine media and yielded aberrant small colonies (SCs). SCVs are usually associated with persistent and relapsing infections (6, 7). During subculture testing, we noted an unexpected feature of the Mu50Ω colony population. In addition to SCs, a few normal-sized colonies (NCs) always appeared conspicuously and consistently in cell populations at a frequency of about 1–3 per 1,000 when Mu50Ω was cultured in vitro (Fig. 1*A*). Here, we introduced the term "normal colony variant" to describe the NC generated from SCV, distinguishing it from the NC of the NC's progeny. Interestingly, NCV progenies were also non-homogeneous. We observed that when NCV was cultured and spread on agar plates, its progenies were mainly NCs (accordingly designated as NCVs); however, SCs were also prevalent in the population at a frequency of about 1–10% in the repeated cultures (Fig. 1*A*). To know the stability of colony compositions of SCV and NCV, each SC and NC culture was passaged in 1:1,000 dilutions for every experiment. We repeated the passage twice a day, continued for 1 wk, and performed a colony count for the cultures each day. The colony count showed that the colony SC/NC ratios had two stable ratios: NC/SC ratios were about 1–3:1,000 for SCV and 90–99:1–10 for NCV. We also failed to isolate any single colony that produced homogeneous colony populations from either the SCV or NCV form of Mu50Ω. The possibility of SCV/NCV reversion being attributable to the replication of existing variants in the inoculating population is excluded by performing repeated colony isolation (plating diluted subcultures and selecting individual colonies) (Fig. 1*A*). Overall, it was evident that there was a bidirectional high-frequent reversion of Mu50Ω colony variants, where SCV emerges from NCV, and vice versa, irrespective of whether the SC or NC was the initial inoculum. The consistency of NC/SC ratios reflects a self-organizing regulatory mechanism of the reversion (see below).

Author contributions: L.C. and K.H. designed research; L.C. and H.-m.N. performed research; L.C. and A.I. analyzed data; and L.C., H.-m.N., A.I., and K.H. wrote the paper.

The authors declare no conflict of interest.

This article is a PNAS Direct Submission.

Freely available online through the PNAS open access option.

[1]To whom correspondence should be addressed. E-mail: longzhu@insti.kitasato-u.ac.jp.

[2]Present address: Research Center for Antiinfectious Drugs, Kitasato Institute for Life Science, Kitasato University, 5-9-1 Shirokane, Minato-ku, Tokyo 108-8641, Japan.

[3]Present address: UKM Medical Molecular Biology Institute, Universiti Kebangsaan Malaysia, 56000 Cheras, Kuala Lumpur, Malaysia.

This article contains supporting information online at www.pnas.org/lookup/suppl/doi:10.1073/pnas.1204307109/-/DCSupplemental.

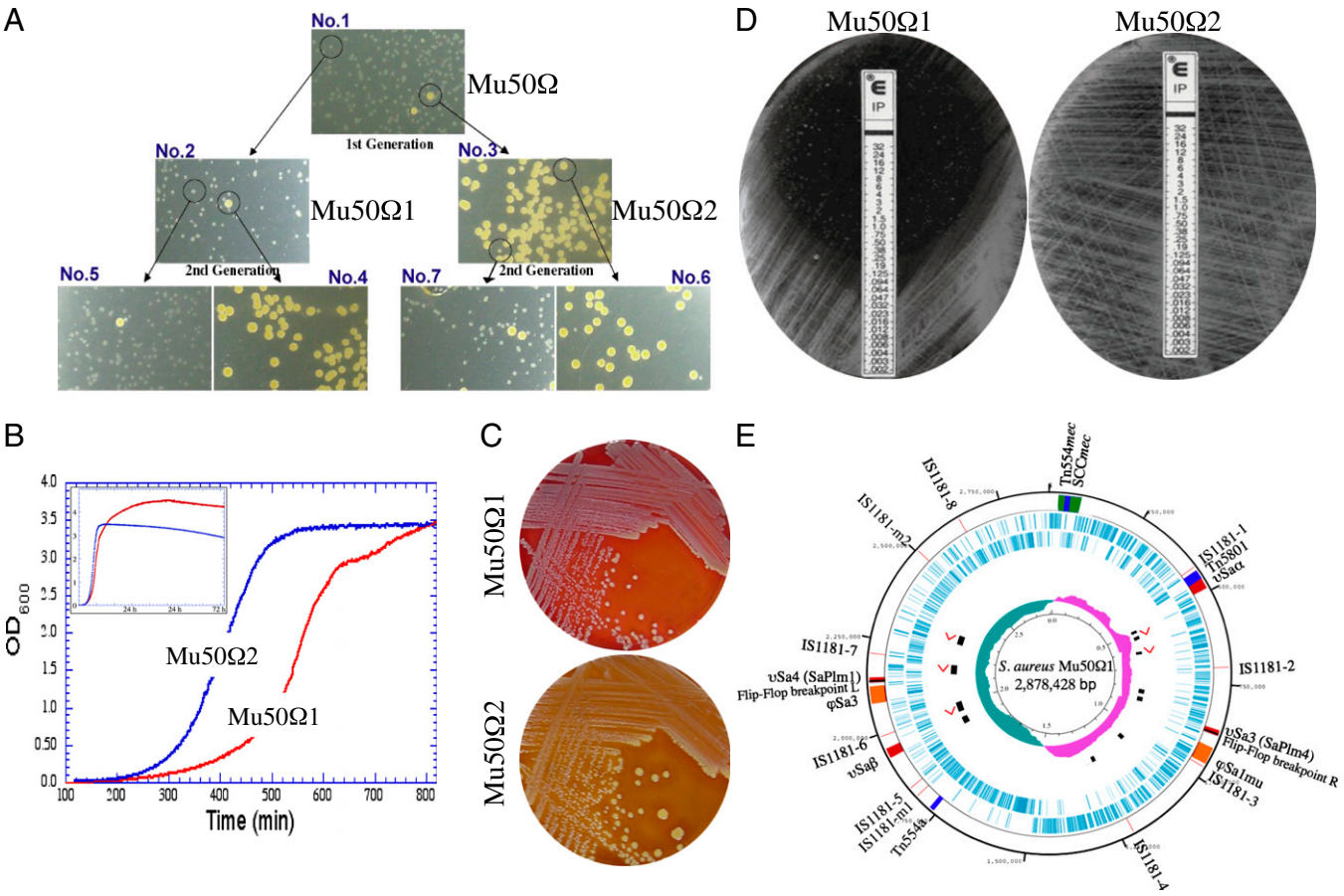

Fig. 1. Characteristics of *S. aureus* Mu50Ω and its derivatives. (*A*, No. 1) Cell populations of MRSA strain Mu50Ω consist of two forms of cells that produce SCs and NCs on agar plates. SC progenies (e.g., Mu50Ω1) were designated as SCV because they produce cell populations that mainly formed SCs with a minor proportion of NCs (NC/SC ratio is about 1–3:1,000). (*A*, No. 2) NC progenies (e.g., Mu50Ω2) were designated as NCV because they produce cell populations that mainly form NCs with a small proportion of SCs (NC/SC ratio is about 90–99:1–10). (*A*, No. 3) Note that the SC and NC can be generated from either NCV or SCV, irrespective of whether SC or NC was the initial inoculum. The Mu50Ω1 exhibited slow growth (*B*), decreased hemolytic activity (*C*), and increased susceptibility to the β-lactam imipenem (*D*), compared with Mu50Ω2. (*E*) Whole-genome sequence of Mu50Ω1 (formerly Mu50Ω) is 2,878,428 bp long, and its genome structure is very similar to that of Mu50. Mu50 was isolated from the same patient as Mu50Ω, and its whole-genome sequence has been determined previously (43). Only 10 SNPs and three short deletions/insertions were identified in a total of 13 genes when the genomes of Mu50 and Mu50Ω were compared, indicating their close relatedness (11). In *E*, the outer circle illustrates the distribution of mobile genetic elements, as indicated. Flip-flop break points are located within the regions of SaPlm4 and SaPlm1 [synonyms: υSa3 and υSa4 (26)]. The second and third circles (blue) illustrate predicted protein-coding regions on the plus and minus strands, respectively. Red arrowheads indicate rRNA and its orientation. Black bars indicate locations of tRNAs. The fifth circle illustrates GC skew. The sixth circle illustrates nucleotide position in megabase pairs (Mbp).

Phenotypic and Functional Properties of the Two Variants. Having established the existence of a reversible reversion between SCV and NCV, we characterized the phenotypic and functional properties of the two variants. We designated Mu50Ω1 as SCV that mainly produced SC progenies with minor frequencies of NC progenies, whereas Mu50Ω2 was designated as NCV that mainly produced NC progenies with minor frequencies of SC progenies. Mu50Ω1 (SCV) showed slow growth (Fig. 1*B*) and less colony pigmentation (Fig. 1 *A* and *C*), and it had impaired hemolytic activity on blood agar (Fig. 1*C*) compared with Mu50Ω2. In addition, Mu50Ω1 was susceptible to β-lactam antibiotics with only a small proportion of resistant cells (resistant cell numbers were almost equal to those of NC), whereas Mu50Ω2 was resistant to β-lactam antibiotics (Fig. 1*D* and Table S1). There was no significant difference in the susceptibilities to other classes of antibiotics tested, except for tetracycline, minocycline, gentamicin, and colistin (Table S1). The SCV Mu50Ω1 showed slightly higher minimum inhibitory concentrations (MICs) of tetracycline and minocycline and lower MICs of gentamicin and colistin, compared with Mu50Ω2 (Table S1). The reason for the discrepancy in aminoglycoside susceptibility of Mu50Ω1 (SCV) from reported SCVs (12–14) in which SCVs usually had high aminoglycoside MICs needed to be clarified.

The transcriptional profiles and phenotypic expression of the phenotypic variants were also analyzed using DNA microarrays (15) and phenotypic arrays (16), respectively. We found that more than 100 genes were differentially expressed between Mu50Ω1 and Mu50Ω2 (Table 1 and Tables S2 and S3) and that their susceptibilities to dozens of chemical compounds were different (Table S4). These differences between SCV and NCV would have a broad impact on bacterial physiology not only in terms of host–pathogen interactions but in bacterial evolutionary processes (see below).

Identification of X-Shaped Chromosome Inversion Between the Two Variants. Phenotypic variation has been discovered in many different bacterial genera belonging to diverse taxonomic groups. The underlying mechanisms for the phenotype variation described so far are genetic or epigenetic alterations at specific genetic loci, including specific gene conversions (17); site-specific inversions (18); insertion-excision processes (19); duplication-deletion of DNA fragments (20, 21); slipped-strand mispairing (22); and epigenetic mechanisms, such as differential methylation (23). However, there are numerous phenotypic switching

Table 1. Representative genes differently expressed in Mu50Ω2 vs. Mu50Ω1

Gene information			
ORF	Name	Product	Ratio (Mu50Ω2/ Mu50Ω1)
Pentose and glucuronate interconversions			
SA0510	araB	Probable L-ribulokinase	1.57
SA0528	—	Hypothetical protein, similar to hexulose-6-phosphate synthase	1.29
SA0529	—	Conserved hypothetical protein	1.25
SA2288	gtaB	UTP-glucose-1-phosphate uridyltransferase	1.83
Amino sugar and nucleotide sugar metabolism			
SA0150	capG	Capsular polysaccharide synthesis enzyme Cap5G	0.33
SA0158	capo	Capsular polysaccharide synthesis enzyme Cap8O	0.43
SA0159	capP	Capsular polysaccharide synthesis enzyme Cap5P	0.68
SA0185	—	Conserved hypothetical protein	0.65
SA0307	—	Conserved hypothetical protein	0.75
SA0457	gcaD	UDP-*N*-acetylglucosamine pyrophosphorylase homolog	1.09
SA0527	nagB	Probable glucosamine-6-phosphate isomerase	1.14
SA0656	nagA	Probable *N*-acetylglucosamine-6-phosphate deacetylase	1.62
SA0693	—	Similar to UDP-*N*-acetylenolpyruvoylglucosamine reductase	1.12
SA1902	murA	UDP-*N*-acetylglucosamine-1-carboxyvinyl transferase 1	2.84
SA1913	mnaA	UDP-GlcNAc 2-epimerase	1.12
SA1926	murZ	UDP-*N*-acetylglucosamine-1-carboxylvinyl transferase 2	1.35
SA1959	glmS	Glucosamine-fructose-6-phosphate aminotransferase	1.73
SA1965	glmM	Phosphoglucosamine-mutase	1.50
SA1999	—	Similar to regulatory protein, SIR2 family	1.84
Oxidative phosphorylation: ATP synthase (complex V)			
SA1904	atpC	FoF1-ATP synthase epsilon subunit	1.49
SA1905	atpD	ATP synthase β-chain	1.79
SA1906	atpG	ATP synthase γ-chain	1.38
SA1907	atpA	ATP synthase α-chain	1.37
SA1908	atpH	ATP synthase δ-chain	1.51
SA1909	atpF	ATP synthase B chain	1.80
SA1910	atpE	ATP synthase C chain	1.88
SA1911	atpB	ATP synthase A chain	1.30
Thiamine metabolism			
SA1894	thiE	Chain B, thiamin phosphate synthase	1.75
SA1895	thiM	Hydroxyethyl thiazole kinase	1.65
SA1896	thiD	Phosphomethylpyrimidine kinase	1.92
SA1897	—	Similar to transcriptional activator TenA	1.58
Vitamin B_6 metabolism			
SA0477	—	Pyridoxine biosynthesis protein	1.17
SA0478	—	Glutamine amidotransferase subunit	1.54
SA0537	—	Pyridoxine kinase	1.26
Biotin metabolism			
SA2211	—	Similar to 6-carboxyhexanoate–CoA ligase	1.98
SA2212	—	Similar to 8-amino-7-oxononanoate synthase	1.41
SA2213	bioB	Biotin synthase	1.65
SA2214	bioA	Adenosylmethionine-8-amino-7-oxononanoate aminotransferase	1.51
SA2215	bioD	Dethiobiotin synthetase	1.21
Ubiquinone and other terpenoid-quinone biosynthesis			
SA0894	—	Similar to 1,4-dihydroxy-2-naphthodate octaprenyltransferase	0.64
SA0895	—	Similar to menaquinone-specific isochorismate synthase	1.43
SA0896	mend	Menaquinone biosynthesis protein	0.54
SA0897	—	Similar to prolyl aminopeptidase (EC 3.4.11.5)	0.45
SA0898	menB	Naphthoate synthase	0.96
SA1303	gerCB	Menaquinone biosynthesis methyltransferase	0.91
SA1614	menC	O-succinylbenzoic acid synthetase	0.83
SA1615	menE	O-succinylbenzoic acid–CoA ligase	1.30

examples in which the mechanism has yet to be elucidated, particularly in cases of switching back to the parental phenotype, as found with Mu50Ω (24).

The identification of stable and reversible phenotype switching between SCV and NCV in Mu50Ω1 and Mu50Ω2 prompted us to extend our study of the genetic mechanism underlying this bidirectional reversion. We began with whole-genome sequencing and a genomic comparison between Mu50Ω1 and Mu50Ω2. The whole-genome sequence of Mu50Ω1 was determined in one of our laboratory projects for studying *S. aureus* glycopeptide resistance in 2008 (11). At that time, we noticed the curious coexistence of a few NCs in the Mu50Ω cell populations, which consisted mainly of SCs. We performed colony purification on drug-free medium, isolated one SC to be established as Mu50Ω,

and applied the strain for whole-genome sequencing. The genome sequence was registered in the DNA Data Bank of Japan (DDBJ) as Mu50Ω (accession no. BABM01000001). At the same time, the NC was also purified and stocked. Therefore, there are actually three Mu50Ω strain series stocked in our laboratory: the original Mu50Ω and two other strains established from SCs and NCs, respectively. In the present study, we have renamed the original isolate Mu50Ω, whereas the strains established from SCs and NCs have been named Mu50Ω1 and Mu50Ω2, respectively. The whole-genome sequence of Mu50Ω2 was determined using the same chromosome-walking method as described for the whole-genome sequencing of Mu50Ω1 (formerly Mu50Ω) (11) (Fig. 1*E*).

Two significant differences were found during the whole-genome comparison. First, we identified a one-nucleotide difference between the Mu50Ω1 (DDBJ accession no. BABM01000001) and Mu50Ω2 genomes in the *sdh* gene (i.e., a G → C transition at nucleotide position 86 that resulted in an Arg29 → Pro29 substitution). Recently, Gaupp et al. (25) reported a study on the *sdh* gene of *S. aureus*, where an in vitro developed *sdh* mutant could show an SCV phenotype, probably attributable to affecting tricarboxylic acid cycle metabolism, and the mutant could be reversed to the wild phenotype by addition of fumarate to the growth medium. However, in the case of Mu50Ω1 and Mu50Ω2, this unique nonsynonymous mutation was not related to the phenotypic difference or the phenotype switching between SCV and NCV. Both SCV and NCV descendants from the same parental strains of either SCV or NCV had the same *sdh* sequence; thus, we categorized this mutation as a progeny-specific event (Fig. 2*A*).

The second and important finding was made when the genomes of Mu50Ω1 and Mu50Ω2 were aligned. We found that almost half of the chromosome (1.26 Mb of 2.87 Mb) was inverted in the Mu50Ω2 genome relative to the Mu50Ω1 genome, exhibiting an "X-shaped" alignment (which we refer to as an X-shaped chromosome inversion) (Fig. 2*B*). This inversion occurred in a region between two oppositely oriented pathogenicity islands, SaPlm4 and SaPlm1 (synonyms: υSa3 and υSa4) (26), located on the left and right replichores and almost symmetrically opposite each other from the origin-terminus replication axis of the chromosome (Fig. 1*E*). We found two copies of 3,638-bp-long sequences with 100% homology that were inversely located at SaPlm4 and SaPlm1, respectively. This sequence was roughly centered in each replichore, and it served as a breakpoint that mediated the X-shaped chromosome inversion. This finding strongly indicates the possibility that the phenotypic differences between Mu50Ω1 and Mu50Ω2 were attributable to the X-shaped chromosome inversion and that this subsequently gave rise to two genome types, type A and type B (Figs. 2*B* and 3*A*).

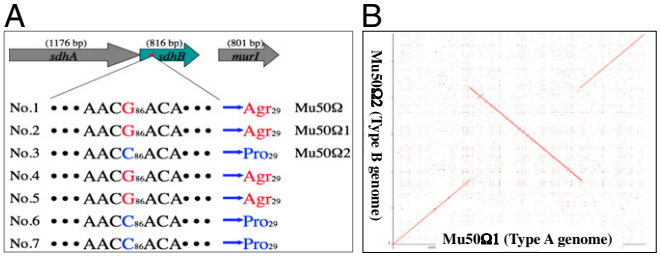

Fig. 2. Comparison of Mu50Ω1 and Mu50Ω2 genomes. (*A*) Nonsynonymous mutation was identified between Mu50Ω1 and Mu50Ω2 in the *sdh* gene (i.e., a G → C transition at nucleotide position 86 that resulted in an Arg29 → Pro29 substitution). This mutation is a progeny-specific event but is not related to the phenotype of SCV or NCV. (*B*) Genome sequence alignment revealed that there was an inversion of a 1,259,709-bp-long genome fragment between Mu50Ω1 and Mu50Ω2 genomes. Strains No. 1 (Mu50Ω), No. 2 (Mu50Ω1), No. 5, and No. 7 are SCV, and strains No. 3 (Mu50Ω2), No. 4, and No. 6 are NCV. Strains No. 4 and No. 5 are progenies of Mu50Ω1, and strains No. 6 and No. 7 are progenies of Mu50Ω2 (Fig. 1*A*).

Reversible X-Shaped Chromosome Inversion Drives Phenotype Switching Between SCV and NCV. Given the symmetrical location of the breakpoints around the origin-terminus axis of the chromosome and the bidirectional nature of the homology recombination process, we hypothesized that the phenotype reversions between SCV and NCV were attributable to a reversible X-shaped chromosome inversion (flip-flop inversion) between type A and type B genomes (Figs. 2*B* and 3*A*). To test the possibility of the flip-flop hypothesis, we first designed four site-specific primer sets to amplify the left and right break-point regions, (F163 and F397 for the type A genome and F600 and F601 for the type B genome) (Figs. 3*B* and 4*A*, I). We successfully amplified all four fragments corresponding to the regions of F163, F397, F600, and F601 from each genome of the Mu50Ω1 and Mu50Ω2 chromosomes (Fig. 4*A*, II). This result strongly indicated that the type A and type B genomes coexist in both SCV and NCV progenies of Mu50Ω. Based on these results, we arrived at the hypothesis that the simultaneous coexistence of two differently arranged genomes (type A and type B) was the only cause for the "colony mixture" phenotype and that the appearance of a Mu50Ω1 or Mu50Ω2 phenotype was dependent on the cell genotype that dominated the total cell population.

This hypothesis was supported by subsequent experiments designed to confirm the association of SCV/NCV phenotype reversion with reversible chromosome inversion. Fig. 4*B*, I shows pulsed-field gel electrophoresis (PFGE) band patterns of Mu50Ω1 and Mu50Ω2 generated by cleaving their genomic DNA with two restriction enzymes, *Asc*I or *SgrA*I. Computer simulations showed that these two enzymes could differentially cut the two genomes and distinguish the type A genome from the type B genome. Interestingly, the band patterns of Mu50Ω1 and Mu50Ω2 were distinguished by an additional band in the Mu50Ω2 genome. In addition, Southern blot hybridization showed that a DNA probe designed to complement a region immediately downstream of fragment F163 in the type A genome and upstream of fragment F601 in the type B genome hybridized to one and two bands in Mu50Ω1 and Mu50Ω2, respectively (Fig. 4*B*, II). The same PFGE results were obtained with all test progenies of Mu50Ω. Thus, all NCV (nos. 3, 4, and 6 of Mu50Ω; Fig. 1*A*) and all SCV (nos. 2, 5, and 7 of Mu50Ω; Fig. 1*A*) progenies shared identical band patterns when their genomic DNA was cut by the enzyme *Sma*I (Fig. 4*C*, I), whereas all NCV progenies produced one extra band compared with the SCV progenies when they were subsequently restricted with the enzyme *Asc*I (Fig. 4*C*, II). This indicates that the extra band found in NCV was a result of the coexistence of cells with type A and B genomes. Given the sensitivity of the Southern blot hybridization methods used in this study, this was consistent with the ratios of the Mu50Ω1 and Mu50Ω2 colony compositions. The genome ratio of the SC (type A genome) to the NC (type B genome) was about 1,000:1–3 for Mu50Ω1 and 1–10:90–99 for Mu50Ω2. Together with the PCR results, it was clear that the type A and type B genomes were responsible for the respective phenotypes of SC and NC and that chromosomal flip-flop inversions were the cause of reversible inversions of the SC and NC types. Finally, simultaneous reversions between SCV and NCV resulted in the appearance of heterogeneous colony phenotypes in Mu50Ω (Fig. 1*A*).

To clarify the association between flip-flop inversion and colony phenotype reversion, we constructed a GFP-reporter gene cassette comprising two components (a tetracycline-inducible *tetO*/*xyl* promoter and a *gfp* reporter). These two components were separately inserted in an inverted direction in the immediate downstream and upstream regions of the right and left flip-flop breakpoints of the Mu50Ω1 type A genome (Fig. 5*A*), respectively, to generate the mutant Mu50Ω1-tetO/xyl-gfp. This construct was designed as a tool to test the X-shaped chromosome inversion hypothesis. Thus, Mu50Ω1-tetO/xyl-gfp

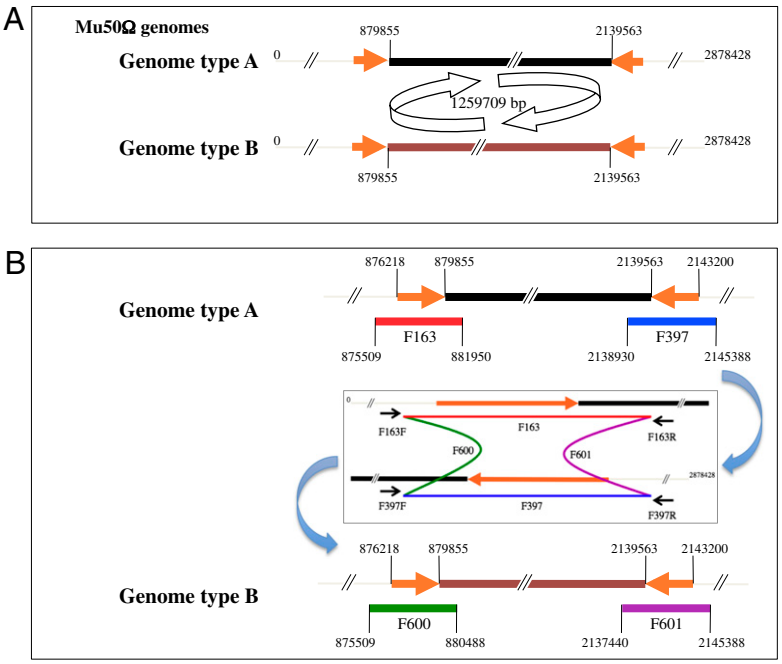

Fig. 3. Illustration of genome inversion between type A and type B genomes of Mu50Ω. (*A*) A 1,259,709-bp-long fragment of 2,878,428 bp of the Mu50Ω genome is reversely inverted to generate either type A or type B genome. (*B*) Inversion occurs through the two break points located at positions 876,218–879,855 and 2,139,563–2,153,200 of the Mu50Ω genome, respectively. Type A and type B genomes can be distinguished by PCR amplification of the fragments F163 and F397 for type A genomes and by PCR amplification of the fragments F600 and F601 for type B genomes. Red arrowheads indicate the fragments of break-point regions and their orientations.

cells could be directly visualized when the inversion occurred by detecting GFP expression that was only present with the X-shaped chromosome inversion (conversion of type A genome to type B to produce the NC) through recombination of the left and right flip-flop breakpoints (Fig. 5*B*). Interestingly, GFP-reporter visualization showed that the SC of Mu50Ω1-tetO/xyl-gfp produced GFP-positive cells at a frequency of about 1 in 1,000, whereas the NC of Mu50Ω1-tetO/xyl-gfp produced about 90% GPF-positive cells (Fig. 5*B*). These observations were consistent with the NC/SC ratio of about 1–3:1,000 for Mu50Ω1, whereas the SC/NC ratio was about 1–10:90–99 for Mu50Ω2. Overall, we can draw the following conclusions:

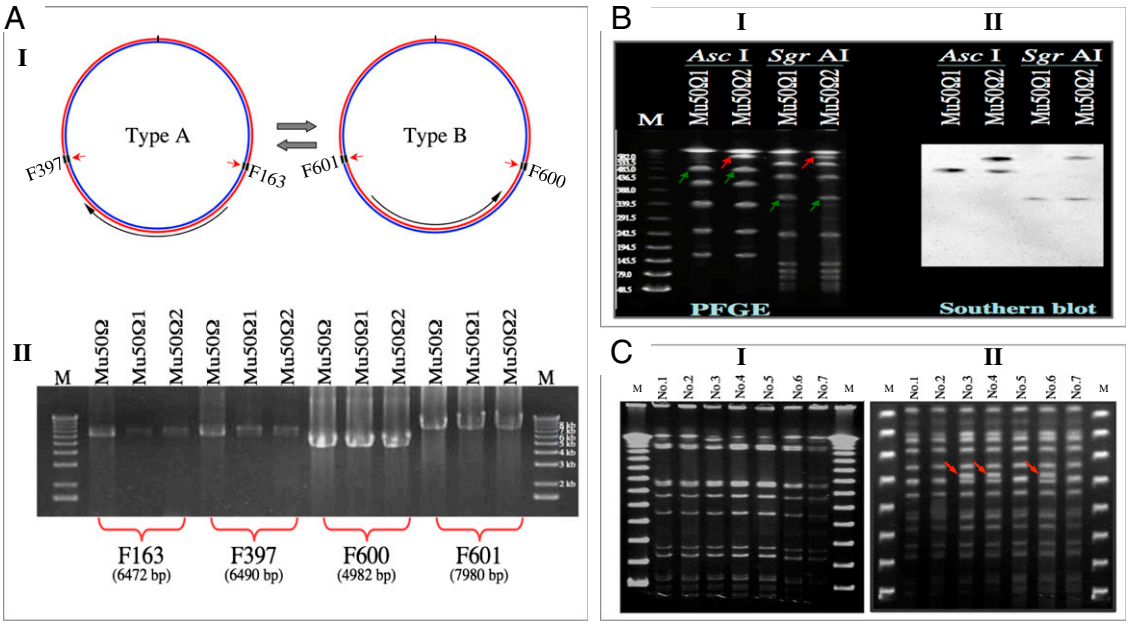

Fig. 4. Coexistence of cells with type A and B genomes in cell populations of both Mu50Ω1 and Mu50Ω2. PCR amplifications of the left and right regions of the inversion breakpoints (*A*, I and Fig. 3*B*) were all positive for genome DNAs from Mu50Ω, Mu50Ω1, and Mu50Ω2 (*A*, II), revealing a simultaneous coexistence of cells with type A and type B (an inverted form of type A) genomes in Mu50Ω1 and Mu50Ω2. (*B*) PFGE pattern and Southern blot results were consistent with those of PCR amplifications. (*B*, I) Two genomes had different PFGE patterns, with an additional band in Mu50Ω2 when its genome was digested with the enzyme *Asc*I or *Sgr*AI. (*B*, II) Southern blotting with specific probes for regions immediately downstream of the right breakpoint of the inversion (Fig. 1*E*) distinguished the two genomes. The PFGE analysis of all Mu50Ω and its derivatives used (Fig. 1*A*) showed that all strains had identical band patterns when their chromosome DNAs were digested by enzyme SmaI (*C*, I), but the band patterns of SCVs and NCVs can be distinguished when the DNAs were further digested by *Asc*I (*C*, II). The green and red arrows in *B* and *C*, indicate PFGE bands that appeared in type A and B genomes, respectively.

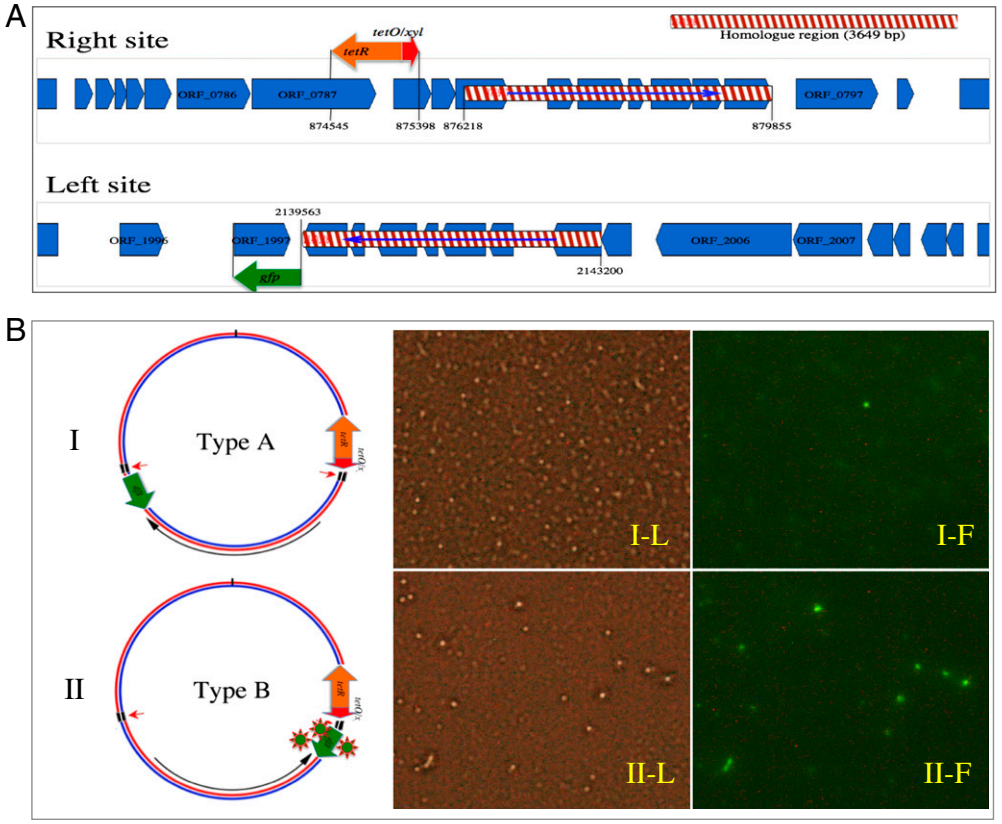

Fig. 5. Confirmation of genome inversion by knocking-in a *gfp*-reporter gene cassette onto the type A genome of Mu50Ω. (*A*) Reporter gene *gfp* with its S/D sequence and tetracycline-inducible promoter *tetO/xyl* are knocked-in separately into the type A genome Mu50Ω chromosome at the left and right flip-flop break points. The red arrow indicates the direction of promoter, and the green arrow indicates the direction of *gfp* transcription. This construct was designed as a tool to test the X-shaped chromosome inversion hypothesis. Thus, Mu50Ω1-tetO/xyl-gfp cells could be directly visualized when the inversion occurred by detecting GFP expression that was only present with the X-shaped chromosome inversion [conversion of type A (*B*, I) genome to type B (*B*, II) to produce NC] through recombination of the left and right flip-flop breakpoints. Determination of GFP expression in a *tetO/xyl/gfp*-cassette knocked-in mutant Mu50Ω1-tetO/xyl-gfp using fluorescence microscopy shows that less than 1% of SC progeny cells (*B*, I-F) and more than 90% of NC progeny cells (*B*, II-F) have GFP expression under tetracycline induction, indicating the occurrence of type A and type B genome inversions during the bacterial growing process. I-L and II-L are light microscopy images, and I-F and II-F are fluorescent microscopy images.

i) Mu50Ω comprises cells with two different genotypes, types A and B, which produce SC and NC, respectively.
ii) SCV and NCV ratios projected by Mu50Ω progenies were a direct result of genotype A/B ratios in the populations. SCV mainly contained type A genome cells (e.g., Mu50Ω1), whereas NCV mainly contained type B genome cells (e.g., Mu50Ω2).
iii) X-shaped chromosome inversion (flip-flop inversion) occurs simultaneously between type A and B genomes.
iv) The flip-flop inversion between type A and B genomes was achieved by homologous recombination between homologous regions of SaPlm4 and SaPlm1 (Figs. 1*E*, 3*A*, and 6).
v) This chromosomal genome inversion can occur frequently during bacterial duplications.

Microarray Transcriptional Analysis. SCV isolates are generally reported to be auxotrophic for compounds that are biosynthesized into components of the electron transport system (10). Menadione and hemin are the two most frequent substances that reverse the *S. aureus* SCV phenotype (27). In addition, thiamine is a cofactor used in menadione biosynthesis (9). Reduced activity of the electron transport system can account for most of the features of the *S. aureus* SCVs; for example, a reduction in available ATP would slow growth, reduce pigment formation, and decrease aminoglycoside transport. Therefore, by down-regulating the biosynthesis of a nonessential pathway, SCVs can change multiple phenotypes that allow the bacterium to survive within the host body and reversal of the SCV phenotype may form the basis for recrudescent infection (27, 28).

To understand the reason why the genome inversion observed in the current study caused NCV vs. SCV phenotype conversion, we carried out a genome-scale transcriptional profile comparison between Mu50Ω1 and Mu50Ω2 (Table 1 and Tables S2 and S3). As shown in Table 1, the most significant alterations apparent in Mu50Ω2 compared with Mu50Ω1 were enhancement (down-regulated in SCV Mu50Ω1) of several genes involved in the metabolism of (*i*) thiamine, (*ii*) oxidative phosphorylation (ATP synthase), (*iii*) vitamin B_6, (*iv*) biotin, (*v*) pentose and glucuronate interconversions, and (*vi*) some amino sugars and nucleotide sugars. Other twofold changed genes are listed in Tables S2 and S3. The possible correlations of the repression of ATP synthesis and thiamin metabolism with the SCV phenotype are well documented (6, 14). However, it is not clear how the other altered gene transcription profiles mentioned above (e.g., vitamin B_6) and biotin metabolism are correlated with the conversion from NCV to SCV phenotype. Vitamin B_6 and biotin are required for a number of important processes in metabolism. They function especially as substrate tethers in decarboxylation reactions in a variety of reactions, including fatty acid synthesis and metabolism and amino acid production, and they serve important roles in the citric acid cycle, one of the main metabolic processes that produce energy (28, 29). The effect of the change in the metabolism of pentose and glucuronate interconversions, amino sugars, and nucleotide sugars on the SCV phenotype

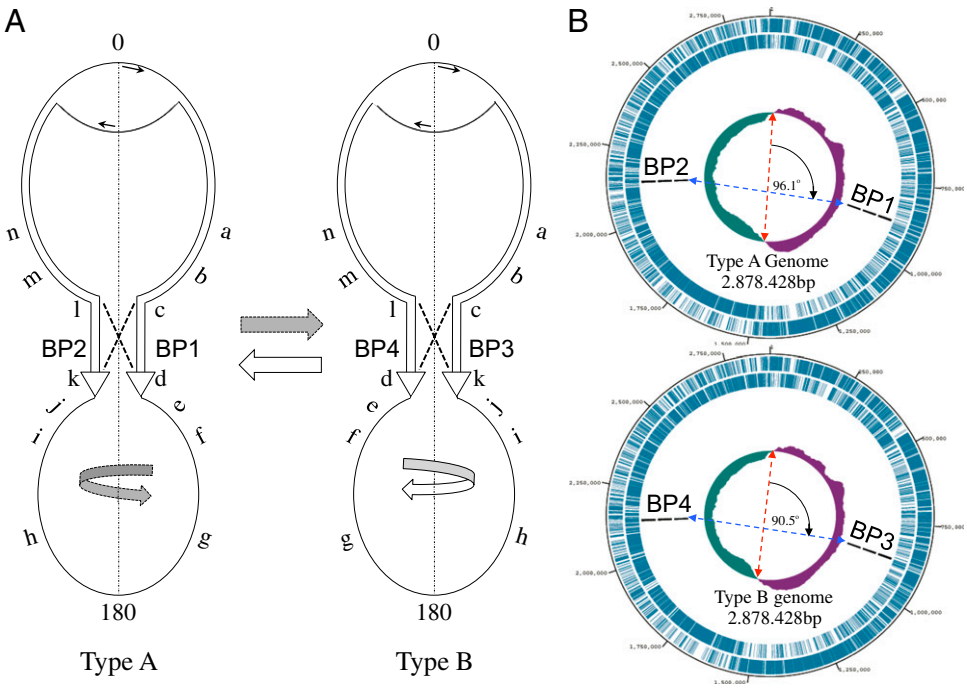

Fig. 6. Illustration of genome inversion through inverted repeat regions (break points) by homolog recombination. (*A*) Type A and type B genomes can be reversibly inverted (flip-flop inversion) at break points (BP1 vs. BP2, BP3 vs. PB4). (*B*) Replication axes of the resulting two genomes, type A and type B, have a difference of 5.9° between each other.

through the energy pathway was also reported elsewhere (30). In addition to these genes, however, there were quite a number of genes involved in cell envelope and cellular processes, and intermediary metabolism up- or down-regulated may involve a pathway of SCV vs. NCV conversion with an as yet unknown mechanism.

SCVs of *S. aureus* can be generated by a variety of genotypic changes and the SCVs resulting from chromosomal inversion presented here is different from the classic SCVs. The classic SCVs are defective in aerobic respiration because of mutations in the respiratory chain, especially in menadione biosynthesis, and the SCV phenotype can be reversed by the addition of menadione to the growth medium (6, 27, 29). It has also been reported that auxotrophy toward hemin, menaquinone, or thymidine is unable to be identified in some SCVs of *S. aureus* and that reversible phenotype reversion from SCV to NCV can be frequently observed; hence, the reasons for the expression of the SCV phenotype and the reversible phenotype reversion remain uncharacterized. Our finding of the genome flip-flop inversion that drives phenotype switching of *S. aureus* provides unique insight into understanding phage variation, underlining the mechanism of SCV generation and its frequent reversion. The strategy of phenotypic switching (large-scale flip-flop inversion) in staphylococci may also be applied for other bacteria.

Phenotype Switching Between the Two Variants Is Self-Organized so as to Maintain Two Heterogeneous Cell Populations. Next, we proceeded to find an explanation for the observation of stable NC and SC ratios in SCV and NCV. When SCV or NCV culture from any growth phase was diluted and plated on agar plates, the NC/SC ratio remained constant at about 1–3:1,000 for SCV and 90–99:1–10 for NCV, regardless of whether we started with NC or SC. Thus, the SC/NC composition ratios in Mu50Ω1 and Mu50Ω2 were constant. However, if only the growth rate is taken into account for the calculation, the number of NCs will soon exceed that of SCs in about 1 d, and the colony ratio balance will be lost even in the case of Mu50Ω1 because the growth rate of NCV is higher than that of SCV (doubling time: 31.21 min for NCV and 38.79 min for SCV) (*SI Materials and Methods*). Therefore, it is highly probable that the regulation of flip-flop inversion plays a critical role in balancing the SC/NC ratios. To prove this, we performed a mathematical analysis. We assumed an exponential growth of the two variants (SCV and NCV) in competition, where they were interchangeable through X chromosome inversion. We denote the appearance frequency of cells carrying a type A genome as y_s and its growth rate as α_s, whereas those of cells carrying the type B genome were denoted as y_n and α_n, respectively. We denoted the reversion rate from NCV to SCV (genotype B to A) as $w_{s\to n}$ and that from SCV to NCV (genotype A to B) as $w_{s\to n}$. Coupled equations for the competitive growth of cells with type A and type B genomes in SCV and NCV during the exponential growth phase are as follows:

$$\frac{dy_s}{dt} = \alpha_s(1-w_{s\to n})y_s + \alpha_n w_{n\to s} y_n,$$
$$\frac{dy_n}{dt} = \alpha_n(1-w_{n\to s})y_n + \alpha_s w_{s\to n} y_s. \quad [1]$$

The asymptotic solution for Eq. **1** shows that if we set all α_s, α_n, $w_{s\to n}$, and $w_{s\to n}$ as invariable values on a bacteria growth time scale, the ratio of y_n to y_s will approach a constant value, whereas bacterial growth reaches the asymptote (*SI Materials and Methods*), irrespective of the initial composition of cells with type A or B genome. However, this obviously contradicted the experimental observations, where the ratio of y_n to y_s in Mu50Ω1 and Mu50Ω2 was different. This indicates that at least one of the values of α_s, α_n, $w_{s\to n}$, or $w_{s\to n}$ takes a different value in Mu50Ω1 and Mu50Ω2. To determine this difference, we first assumed that the basic growth rates, α_s and α_n, were constant when finding the values of $w_{s\to n}$, and $w_{s\to n}$ by fitting the experimental growth curves for Mu50Ω1 and Mu50Ω2 simultaneously.

The fitting was conducted using a generalized form of the Lotka–Volterra equation (*SI Materials and Methods*), where the effects of the flip-flop probability, saturation property, and bacterial degradation were included. Moreover, we used a simplified assumption that Mu50Ω1 and Mu50Ω2 shared the same $w_{s\to n}$ value. With a constant and very small value for the NC/SC ratios, the $w_{s\to n}$ value for Mu50Ω1 was predicted to be very small. Otherwise, the observed colony ratios will not be constant even if we set $w_{s\to n}$ at a maximum value of 1.0. Moreover, when the $w_{s\to n}$ value was small, increasing its value by several orders of magnitude did not greatly change the growth pattern of Mu50Ω2, which validates the use of the same $w_{s\to n}$ value for both Mu50Ω1

and Mu50Ω2. We should also point out that it was impossible to fix the absolute values of $w_{s\to n}$ and $w_{s\to n}$, because either increasing or decreasing both values appropriately had no net effect. Fig. 7 shows the fitting results. By setting the value of $w_{s\to n}$ as 3×10^{-5} for both Mu50Ω1 and Mu50Ω2, we finally obtained $w_{s\to n}$ values of 0.25 for Mu50Ω1 and 0.02 for Mu50Ω2. A significant finding of the mathematical analysis was that the flip-flop probabilities ($w_{s\to n}$ values) of Mu50Ω1 and Mu50Ω2 must take different values when implementing the best fit, indicating that reversion rates driven by genome flip-flop inversions are explicitly asymmetrical for Mu50Ω1 and Mu50Ω2 (*SI Materials and Methods*). This asymmetry of the flip-flop probability is inevitable for both Mu50Ω1 and Mu50Ω2 to maintain constant NC/SC ratios, thereby generating two stable cell populations. This appears to be a self-organizing process for stabilizing the two Mu50Ω variants, SCV and NCV, with different SC/NC ratios, which are represented by Mu50Ω1 and Mu50Ω2, respectively.

The bistable nature of Mu50Ω in terms of its production of the two variants, SCV and NCV, and when balancing the flip-flop inversion that maintains the two stable colony ratios of SC/NC for SCV (Mu50Ω1) and NCV (Mu50Ω2) may confer fitness advantage when responding to changing environments, thereby functioning as a bet-hedging strategy. For example, SCVs facilitate escape from immune attacks, whereas NCVs are resistant to antibiotic treatment during infection.

Overall, our findings indicate that a bidirectional phenotype reversion is driven by large-scale genome flip-flop inversion. This self-organized control of inversion provides unique insights into genome evolution and its flexible organization, particularly the process of bistable heterogeneous cell populations. This may lead to a better understanding of pathogen population dynamics and selection on the architecture of circular bacterial chromosomes.

Enhanced *recA* Expression Seems to Be Associated with SCV Reversion from NCV in Mu50Ω. Although the detailed mechanism underlying the control of the asymmetrical inversion process in Mu50Ω1 and Mu50Ω2 remains to be clarified, the involvement of a *recA*-mediated homologous recombination pathway (31) is strongly suggested.

The phenotype reversion between NCV and SCV of Mu50Ω linage is attributable to the genome flip-flop inversion, and this inversion is asymmetrical between the two variants. The reversion probability of SCV from NCV is about 10-fold higher in Mu50Ω1 than Mu50Ω2 (see above). To understand the regulatory mechanism of this reversion, we first determined the level of *recA* gene expression. The RecA protein promotes pairing between an ssDNA molecule and a homologous sequence in another DNA molecule, which plays a central role in the recombination pathway of the bacteria (32). Because it is an important protein in bacterial homolog recombination, we determined its expression level by quantitative PCR and found that Mu50Ω1 ($w_{s\to n}$ value of 0.25) had a significantly higher level of *recA* expression compared with Mu50Ω2 ($w_{s\to n}$ value of 0.02) (Fig. 8*A*). The calculation showed that *recA* expression in Mu50Ω1 was 26.56%, 15.15%, and 15.03% higher than in Mu50Ω2 when the expression level was normalized with that of reference genes 16S-rRNA1, *gyrB*, and *pta*, respectively. This supports the results that reversion probability of SCV from NCV is 10-fold higher in Mu50Ω1 than Mu50Ω2. Overall, the asymmetrical flip-flop inversion between Mu50Ω1 and Mu50Ω2 seems to be associated with the *recA*-mediated homolog recombination pathway. To clarify this observation further, we constructed tetracycline-inducible expression vector pLC1 (Fig. 9) and used this vector to generate *recA*-expression vector pLC1-*recA*, followed by overexpression of *recA* in genotype B cells of Mu50Ω2. The results showed that induced overexpression of *recA* using anhydrotetracycline significantly increased the phenomenon of NC to SC phenotype conversion by about threefold (Fig. 8*B*). In addition, because our trials (performed 3 times) to construct a *recA* KO mutant failed for unknown reasons, we carried out plasmid-mediated *recA* antisense overexpression in

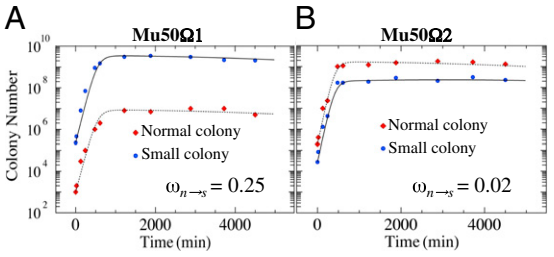

Fig. 7. Asymmetrical probabilities of genome flip-flop inversions in Mu50Ω1 and Mu50Ω2. Growth curves of Mu50Ω1 and Mu50Ω2 in the batch cultures are shown as a function of time. The points shown with blue circles and red diamonds indicate the number of cells with type A and type B genomes, respectively. The solid and dotted lines are the calculations with generalized Lotka–Volterra equations applied to the competitive growth of bacteria with type A and type B genomes, where the optimal values of the parameters are chosen to fit the experimental data (*SI Materials and Methods*). Note that the ratio of cell number with type A to type B genome is almost constant for both Mu50Ω1 and Mu50Ω2 and that the reversion rate from NCV to SCV ($w_{s\to n}$) is 12.5-fold higher in Mu50Ω1 compared with Mu50Ω2.

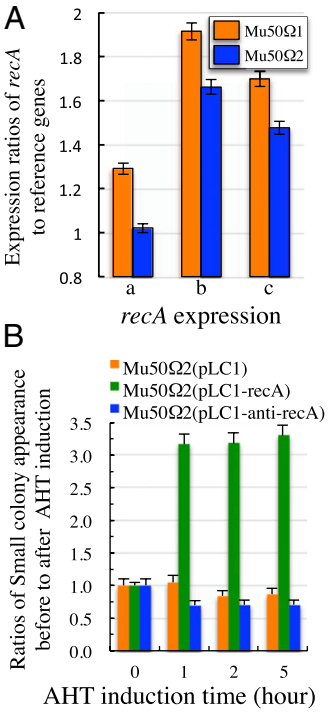

Fig. 8. Overexpression of *recA* increases the rate of NCV to SCV conversion. (*A*) Expression level of *recA* was normalized with the expression level of genes 16S-rRNA1 (a), *gyrB* (b), and *pta* (c), respectively. Data shown are three independent determinations with double-set experiments. Note that *recA* was highly expressed in Mu50Ω1 compared with Mu50Ω2. To study the impact of *recA* on the reversion between SCV and NCV, the whole *recA* and its 522-bp-long antisense fragment with the covering promoter region were cloned under *tetO/xyl* promoter of pLC1 (Fig. 9) to construct pLC1-recA and pLC1-anti-recA. The resulting vectors were introduced into Mu50Ω2 cells of genome type B to test the conversion rate from NCV to SCV in comparison to the control strain, which was introduced in control vector pLC1. (*B*) Note that although overexpression of *recA* antisense reduced the rate of NCV to SCV conversion slightly, the overexpression of *recA* increased the rate of NCV to SCV conversion about threefold, indicating an association between genome inversion and the *recA* expression level. Data shown are from three independent experiments. AHT, anhydrotetracycline.

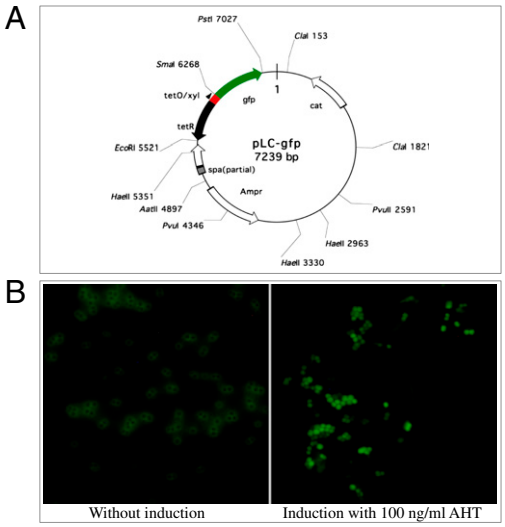

Fig. 9. Efficiency of constructed tetracycline-inducible *E. coli*/*S. aureus* shuttle vector pLC1. A tetracycline-inducible shuttle vector pLC1 was constructed, and its inducing efficiency was determined by inserting *gfp* genes under the *tetO*/*xyl* promoter. The constructed pLC-gfp vector (*A*) was introduced into MRSA strain N315 to generate N315(pLC-gfp), and the *tetO*/*xyl* promoter efficiency was evaluated by detecting the GPF expression level under fluorescent microscopy after induction with 100 ng/mL anhydrotetracycline (AHT) (*B*). Note that GFP was significantly produced under induction with 100 ng/mL AHT.

B-form cells of Mu50Ω2 to evaluate the impact of *recA* on the flip-flop inversion. Contradictory to the *recA* overexpression, *recA* antisense overexpression reduced the ratio of the conversion from NC to SC phenotype slightly, which supports the results of *recA* overexpression (Fig. 8*B*). Taken together, our results support the above suggestion that the *recA* system plays an important role in maintaining the asymmetrical flip-flop inversion and bistable nature of Mu50Ω colony phenotypes. However, the detailed pathway(s) by which it regulates the asymmetrical flip-flop inversion between two variants remains to be elucidated.

Materials and Methods

Clinical Case and Bacterial Strains. Mu50Ω is a methicillin-resistant *S. aureus* (MRSA) strain isolated from a male newborn with pulmonary atresia who had been hospitalized for surgery four times for a total of 20 mo from January 1996 to December 1998 as a result of the repeated surgical incision site infections by *S. aureus* (33, 34). The clinical course and detailed information about bacterial isolates used in this study are described in *SI Materials and Methods*.

Colony Morphology and Assessment of NC/SC Ratio. Ten microliters of an overnight tested bacterial culture was inoculated into 10 mL of fresh brain heart infusion (BHI) broth and cultured at 37 °C with gentle shaking in a photorecording incubator (TN-2612; ADVANTEC). The bacterial culture at exponential growth phase (OD_{600} around 1) was used to carry out 10-fold serial dilutions in 0.9% saline, and 0.1 mL of each dilution was spread onto Brain Heart Infusion (BHI) or Mueller-Hinton (MH) agar plates. The plates were then incubated at 37 °C, and the colony morphology was observed after 24- and 48-h incubations. The NC/SC ratio was calculated by counting the number of colony appeared on the agar plates.

Antimicrobial Susceptibility Testing. The MIC for various antibiotics was measured using E-test strips (AB BIODISK). A sterile cotton swab was immersed in 0.5 Mcfarland of tested bacterial culture before streaking on sterile Mueller–Hinton agar plates. The antimicrobial strips were applied after 10 min. Plates were then incubated at 37 °C, and results were read after 24 and 48 h.

Bacterial Growth Curve and Doubling Time. Overnight culture of a tested strain was diluted 1:1,000 in 10 mL of fresh BHI broth and grown at 37 °C with gentle shaking in a photorecording incubator (TN-2612). The OD_{600} was monitored automatically every 2 min, and the growth rates of tested strains were observed over the intended time frame. Doubling times in the exponential growth phase were calculated as follows: Doubling time equals $[(t_2 - t_1) \times \log 2]/[\log(OD_{600})$ at $t_2 - \log(OD_{600})$ at $t_1]$, where t_1 and t_2 are the times of measurement (35).

Phenotype Microarray Assays. Phenotype microarray analysis was carried out using the OmniLog system (36). Strains to be tested were plated on Biolog Universal Growth medium plus blood agar plates and incubated overnight at 37 °C. Cells were swabbed from the plates after overnight growth and suspended in appropriate medium containing Dye Mix C; 100 μL of a 1:200 dilution of an 85% transmittance suspension of cells was added to each well of the Phenotype Microarray (PM) plates. Plates were incubated in the OmniLog for 48 h with readings taken every 15 min. Data analysis was performed using Kinetic and Parametric software (Biolog). Phenotypes were determined based on the area difference under the kinetic curve of dye formation between the two strains to be tested.

PFGE and Southern Blot Hybridization. PFGE with SmaI-cut genomic DNA was carried out as described previously (37), using a CHEF DRII apparatus (Bio-Rad Laboratories) with an electric field strength of ~6 V/cm and a pulse time of 20 s for 22 h. To differentiate the restriction profile of the genomes of Mu50Ω1 from Mu50Ω2, enzyme *Asc*I or *Sgr*AI was used for DNA digestion. Southern blotting hybridization was carried out as described previously (37). The DNA probe was prepared using primers SAV0813-Fp22 (5′-TTAACTATGAGCACGCTATT-3′) and SAV0813-Rp468 (5′-GGTTTGCGTAGTAATGAAGT-3′), which amplified 449-bp DNA fragments of unique regions located just downstream of the left flip-flop breakpoint in type A genome or just upstream of the right flip-flop breakpoint in type B genome (Figs. 1*E* and 4*A*). The probes were then labeled with digoxigenin using a DNA labeling kit (Roche). Visualization of digoxigenin-labeled DNA was performed using a chemiluminescent substrate kit (CSPD; Roche), and the band was analyzed under an ImageQuant LAS 4000 (GE Healthcare) image analyzer.

Chromosomal DNA Extraction, DNA Manipulation, Nucleotide Sequencing, and Bacterial Electroporation. *S. aureus* chromosomal DNA isolations were performed using phenol/chloroform extraction and precipitated with ethanol as described previously (15). PCR amplifications were carried out using a Takara Thermal Cycler with conditions recommended by the manufacturer. Nucleotide sequencing was carried out via fluorescence dideoxy chain termination chemistry with a BigDye Terminator v3.1 Cycle Sequencing Kit (Applied Biosystems) and an ABI Prism 3100 genetic analyzer (Applied Biosystems). Plasmid DNA was isolated from *Escherichia coli* using a Quantum Prep Miniprep Kit (Bio-Rad Laboratories) according to the manufacturer's instructions. Restriction endonuclease digestion, ligation reactions, and DNA cloning were carried out in accordance with the manufacturer's instructions. Electroporation of *S. aureus* was performed with a Bio-Rad Gene Pulser (Bio-Rad Laboratories) with a pulse controller as described previously (38).

Whole-Genome Sequencing. The whole-genome sequence of Mu50Ω2 was determined using the same chromosome-walking method as described for the whole-genome sequencing of Mu50Ω1 (formerly Mu50Ω; DDBJ accession no. BABM01000001) (11). Briefly, a total of 533 overlapping PCR fragments (mean length about 6 kb) that cover the whole Mu50Ω1 genome were PCR-amplified with Mu50Ω2 chromosomal DNA as the template, and each fragment was sequenced by primer-walking. The whole Mu50 genome sequence was used as a genome scaffold for primer design as well as orientation of the contiguous PCR fragments of Mu50Ω2.

RNA Preparation and Microarray Analysis. Preparation of microarray chips with whole *S. aureus* N315 chromosome ORFs and transcriptional profile analysis were carried out as described previously (15). Bacterial culture, RNA extraction, cDNA labeling, hybridization, and data analysis for microarray analysis were carried out according to protocols described previously (15, 39).

Quantitative PCR. Comparison of recA gene expression between the Mu50Ω1 and Mu50Ω2 was carried out using the GenomeLab GeXP genetic analysis system (Beckman Coulter) according to the protocol provided. Detailed procedures about mRNA determination and normalization are provided in *SI Materials and Methods*.

Knock-In of a Reporter Gene Cassette into Mu50Ω1 Chromosome. To monitor genome flip-flop reversion, using gene replacement strategy (40, 41), a reporter gene *gfp* with an S/D sequence and tetracycline-inducible promoter

tetO/xyl (42) were knocked-in separately into Mu50Ω1 chromosome at the left and right flip-flop break points. Detailed procedures are provided in *SI Materials and Methods*.

Construction of Tetracycline-Inducible *E. coli/S. aureus* Shuttle Vector pLC1. The pRIT5dS-graFp-gfp shuttle vector (15) was reconstructed to develop pLC1. The *graF* promoter of pRIT5dS-graFp-gfp was replaced with tetracycline-inducible tetO/xyl promoter originating from pWH353 (42) to establish pRIT5dS-tetO/xyl-gfp. The inducible activity of tetO/xyl promoter of pRIT5dS-tetO/xyl-gfp was confirmed by a tetracycline-inducing experiment after introducing the pRIT5dS-tetO/xyl-gfp into MRSA N315. The *gfp* was then removed from pRIT5dS-tetO/xyl-gfp to establish pLC1, which carries tetracycline-inducible promoter tetO/xyl-gfp upstream of the multicloning site (MCS) in which the cut sites for SmaI, SalI, PstI, and NheI were available. Constructed plasmids were partially sequenced for sequence validation of MCS and *tetO/xyl* promoter. The stability of plasmid pLC1 in *S. aureus* was determined by passaging the plasmid in antibiotic-containing medium five times.

Overexpression of *recA* and Its Antisense. To overexpress *recA*, plasmid pLC1-recA was constructed by cloning *recA* ORF into the SmaI and PstI cut sites of the MCS on pLC1 to generate pLC1-recA. For cloning antisense-*recA*, a 522-bp-long PCR fragment of *recA* (position at −150 to +372) was inversely inserted into the SmaI and PstI cut sites of pLC1 to develop pLC1–anti-recA. The regions covering MCS and *tetO/xyl* were sequenced for sequence validation. The constructed plasmids were then introduced into Mu50Ω2, and overexpression of the insertions were studied as described elsewhere (15).

ACKNOWLEDGMENTS. We thank Dr. Fumihilko Takeuchi and Dr. Barry Bochner for their scientific discussions and assistance with the phenotype microarray (PM) array. This work was supported by Grant-in-Aid S0991013 from the Ministry of Education, Science, Sports, Culture, and Technology of Japan for the Foundation of Strategic Research Projects in Private Universities and partially by Grant-in-Aid for Scientific Research 23570009 (to L.C.) from the Ministry of Education, Science, Sports, Culture, and Technology of Japan.

1. van der Woude MW, Bäumler AJ (2004) Phase and antigenic variation in bacteria. *Clin Microbiol Rev* 17:581–611.
2. Kussell E, Leibler S (2005) Phenotypic diversity, population growth, and information in fluctuating environments. *Science* 309:2075–2078.
3. Fraser C, Alm EJ, Polz MF, Spratt BG, Hanage WP (2009) The bacterial species challenge: Making sense of genetic and ecological diversity. *Science* 323:741–746.
4. Kussell E, Kishony R, Balaban NQ, Leibler S (2005) Bacterial persistence: A model of survival in changing environments. *Genetics* 169:1807–1814.
5. Avery SV (2006) Microbial cell individuality and the underlying sources of heterogeneity. *Nat Rev Microbiol* 4:577–587.
6. Proctor RA, et al. (2006) Small colony variants: A pathogenic form of bacteria that facilitates persistent and recurrent infections. *Nat Rev Microbiol* 4:295–305.
7. van den Broek D, Bloemberg GV, Lugtenberg B (2005) The role of phenotypic variation in rhizosphere Pseudomonas bacteria. *Environ Microbiol* 7:1686–1697.
8. von Eiff C (2008) Staphylococcus aureus small colony variants: A challenge to microbiologists and clinicians. *Int J Antimicrob Agents* 31:507–510.
9. Tuchscherr L, et al. (2010) Staphylococcus aureus small-colony variants are adapted phenotypes for intracellular persistence. *J Infect Dis* 202:1031–1040.
10. von Eiff C, et al. (1997) A site-directed Staphylococcus aureus hemB mutant is a small-colony variant which persists intracellularly. *J Bacteriol* 179:4706–4712.
11. Cui L, Neoh HM, Shoji M, Hiramatsu K (2009) Contribution of *vraSR* and *graSR* point mutations to vancomycin resistance in vancomycin-intermediate *Staphylococcus aureus*. *Antimicrob Agents Chemother* 53:1231–1234.
12. Chuard C, Vaudaux PE, Proctor RA, Lew DP (1997) Decreased susceptibility to antibiotic killing of a stable small colony variant of Staphylococcus aureus in fluid phase and on fibronectin-coated surfaces. *J Antimicrob Chemother* 39:603–608.
13. Massey RC, Buckling A, Peacock SJ (2001) Phenotypic switching of antibiotic resistance circumvents permanent costs in Staphylococcus aureus. *Curr Biol* 11:1810–1814.
14. Proctor RA, et al. (1998) Staphylococcal small colony variants have novel mechanisms for antibiotic resistance. *Clin Infect Dis* 27(Suppl 1):S68–S74.
15. Cui L, Lian JQ, Neoh HM, Reyes E, Hiramatsu K (2005) DNA microarray-based identification of genes associated with glycopeptide resistance in *Staphylococcus aureus*. *Antimicrob Agents Chemother* 49:3404–3413.
16. Bochner BR (2003) New technologies to assess genotype-phenotype relationships. *Nat Rev Genet* 4:309–314.
17. Hill SA, Woodward T, Reger A, Baker R, Dinse T (2007) Role for the RecBCD recombination pathway for pilE gene variation in repair-proficient Neisseria gonorrhoeae. *J Bacteriol* 189:7983–7990.
18. Krinos CM, et al. (2001) Extensive surface diversity of a commensal microorganism by multiple DNA inversions. *Nature* 414:555–558.
19. Higgins BP, Carpenter CD, Karls AC (2007) Chromosomal context directs high-frequency precise excision of IS492 in Pseudoalteromonas atlantica. *Proc Natl Acad Sci USA* 104:1901–1906.
20. Waite RD, Penfold DW, Struthers JK, Dowson CG (2003) Spontaneous sequence duplications within capsule genes cap8E and tts control phase variation in Streptococcus pneumoniae serotypes 8 and 37. *Microbiology* 149:497–504.
21. Vial L, et al. (2006) Phase variation and genomic architecture changes in Azospirillum. *J Bacteriol* 188:5364–5373.
22. Davidsen T, Tønjum T (2006) Meningococcal genome dynamics. *Nat Rev Microbiol* 4:11–22.
23. Henderson IR, Owen P, Nataro JP (1999) Molecular switches—The ON and OFF of bacterial phase variation. *Mol Microbiol* 33:919–932.
24. Wisniewski-Dyé F, Vial L (2008) Phase and antigenic variation mediated by genome modifications. *Antonie van Leeuwenhoek* 94:493–515.
25. Gaupp R, Schlag S, Liebeke M, Lalk M, Götz F (2010) Advantage of upregulation of succinate dehydrogenase in Staphylococcus aureus biofilms. *J Bacteriol* 192:2385–2394.
26. Novick RP, Subedi A (2007) The SaPIs: Mobile pathogenicity islands of Staphylococcus. *Chem Immunol Allergy* 93(1):42–57.
27. Lannergård J, et al. (2008) Identification of the genetic basis for clinical menadione-auxotrophic small-colony variant isolates of Staphylococcus aureus. *Antimicrob Agents Chemother* 52:4017–4022.
28. McNamara PJ, Proctor RA (2000) Staphylococcus aureus small colony variants, electron transport and persistent infections. *Int J Antimicrob Agents* 14:117–122.
29. Kaplan ML, Dye W (1976) Growth requirements of some small-colony-forming variants of Staphylococcus aureus. *J Clin Microbiol* 4:343–348.
30. Chatterjee I, et al. (2009) Staphylococcus aureus ClpC ATPase is a late growth phase effector of metabolism and persistence. *Proteomics* 9:1152–1176.
31. Reiss B, et al. (2000) RecA stimulates sister chromatid exchange and the fidelity of double-strand break repair, but not gene targeting, in plants transformed by Agrobacterium. *Proc Natl Acad Sci USA* 97:3358–3363.
32. Camerini-Otero RD, Hsieh P (1995) Homologous recombination proteins in prokaryotes and eukaryotes. *Annu Rev Genet* 29:509–552.
33. Hiramatsu K, et al. (1997) Methicillin-resistant *Staphylococcus aureus* clinical strain with reduced vancomycin susceptibility. *J Antimicrob Chemother* 40:135–136.
34. Cui L, Murakami H, Kuwahara-Arai K, Hanaki H, Hiramatsu K (2000) Contribution of a thickened cell wall and its glutamine nonamidated component to the vancomycin resistance expressed by Staphylococcus aureus Mu50. *Antimicrob Agents Chemother* 44:2276–2285.
35. Cui L, et al. (2003) Cell wall thickening is a common feature of vancomycin resistance in Staphylococcus aureus. *J Clin Microbiol* 41:5–14.
36. Bochner BR, Gadzinski P, Panomitros E (2001) Phenotype microarrays for high-throughput phenotypic testing and assay of gene function. *Genome Res* 11:1246–1255.
37. Yoshida T, Kondo N, Hanifah YA, Hiramatsu K (1997) Combined use of ribotyping, PFGE typing and IS431 typing in the discrimination of nosocomial strains of methicillin-resistant *Staphylococcus aureus*. *Microbiol Immunol* 41:687–695.
38. Kuwahara-Arai K, Kondo N, Hori S, Tateda-Suzuki E, Hiramatsu K (1996) Suppression of methicillin resistance in a mecA-containing pre-methicillin-resistant Staphylococcus aureus strain is caused by the mecI-mediated repression of PBP 2′ production. *Antimicrob Agents Chemother* 40:2680–2685.
39. Cui L, et al. (2010) An RpoB mutation confers dual heteroresistance to daptomycin and vancomycin in Staphylococcus aureus. *Antimicrob Agents Chemother* 54:5222–5233.
40. Bae T, Schneewind O (2006) Allelic replacement in Staphylococcus aureus with inducible counter-selection. *Plasmid* 55(1):58–63.
41. Neoh HM, et al. (2008) Mutated response regulator graR is responsible for phenotypic conversion of Staphylococcus aureus from heterogeneous vancomycin-intermediate resistance to vancomycin-intermediate resistance. *Antimicrob Agents Chemother* 52:45–53.
42. Geissendörfer M, Hillen W (1990) Regulated expression of heterologous genes in Bacillus subtilis using the Tn10 encoded tet regulatory elements. *Appl Microbiol Biotechnol* 33:657–663.
43. Kuroda M, et al. (2001) Whole genome sequencing of methicillin-resistant Staphylococcus aureus. *Lancet* 357:1225–1240.

Supporting Information

Cui et al. 10.1073/pnas.1204307109

SI Materials and Methods

Clinical Case and Bacterial Strains. Mu50Ω is a methicillin-resistant *Staphylococcus aureus* (MRSA) strain isolated from the same patient from whom the first vancomycin-intermediate *S. aureus* Mu50 was isolated (1, 2). The patient, a male newborn with pulmonary atresia, had been hospitalized for a total of 20 mo four times from January 1996 to December 1998 for surgery attributable to the repeated surgical incision site infections by *S. aureus*. Mu50 was isolated in September 1996 during the patient's first hospitalization (1), and Mu50Ω was isolated in December 1997 at his third hospitalization (3). On his third hospitalization, an abscess under the sternum, just beneath the original surgical incision site, grew multiple MRSA colonies on agar plates. They (10 colonies were tested) had identical pulsed-field gel electrophoresis patterns, and the vancomycin minimum inhibitory concentration (MIC) for all but one showed the same MIC as for Mu50 (8 mg/L). This exceptional colony was small in size and had a vancomycin MIC of 0.5 mg/L. Therefore, this strain was considered to be a derivative of Mu50 and was designated as Mu50Ω. By reviewing the clinical records, it was noted that the patient had 54 positive cultures for *S. aureus* during a total of 87 bacterial examinations over the course of the whole hospitalization period. The records also described occasional observations of "tiny-sized" colony isolates from the specimens taken from the infectious site of the patient, but they had not been characterized or stocked for further study except for Mu50Ω. Thereafter, in our sequential genome comparison studies, it was shown that there were only 10 SNPs and three mismatches between the Mu50 and Mu50Ω genomes (3), revealing a close genetic relatedness of Mu50 and Mu50Ω. The whole-genome sequences of Mu50 and Mu50Ω were disclosed in the GenBank (accession no. BA000017) and in the DNA Data Bank of Japan (accession no. BABM01000001). The bacterial strains were stocked in brain heart infusion (BHI) broth with 40% (vol/vol) glycerol at −70 °C at the time of isolation. Unless stated, all bacterial precultures were done with BHI broth and cultured overnight with shaking at 37 °C.

Quantitative PCR. A comparison of *recA* gene expression between the Mu50Ω1 and Mu50Ω2 was carried out using the GenomeLab GeXP genetic analysis system from Beckman Coulter. Total RNA quantity and quality were assessed using a Nanodrop spectrophotometer (Nanodrop Technologies). The quantitative PCR assay was carried out using the GenomeLab GeXP Start Kit (Beckman Coulter) according to the protocol provided. First, an RT reaction was carried out in a 20-μL total volume containing 1× RT buffer, the reverse primer mixtures at 50 nM each, 20 units of reverse transcriptase, 5 μL of the kanamycin resistance gene (kna) RNA (positive control), and 50 ng of the sample RNA. The final volume was brought to 20 μL with DNase/RNase-free H_2O. This reaction mixture was incubated with the following program: 1 min at 48 °C, 5 min at 37 °C, 1 h at 42 °C, and 5 min at 95 °C. Second, a PCR assay was carried out with the mixture containing, at the final concentration, 1× PCR buffer, 1.25 mM $MgCl_2$, the forward primer mixtures at 20 nM each, 3.5 units of the thermo-Start DNA polymerase (ABgene AB-0908/A), and 9.3 μL of the cDNA from the RT reaction. The cycle parameters were 10 min at 95 °C and 35 cycles of 30 s at 94 °C, 30 s at 55 °C, and 1 min at 68 °C. The resulting samples were diluted 10 times, added in a 96-well microplate with the DNA size standard-400, and analyzed on the GenomeLab GeXP genetic analysis system. The expression levels of the 16S-rRNA1 were used to normalize for variation in total cDNA concentration, and the *recA* gene expression was evaluated by normalizing with the levels of 16S-rRNA1, *graB*, and *pta* genes.

Knock-In of a Reporter Gene Cassette into Mu50Ω1 Chromosome. To monitor genome flip-flop reversion, a reporter gene *gfp* with its S/D sequence and tetracycline-inducible promoter *tetO/xyl* were knocked-in separately into Mu50Ω1 chromosome at the left and right flip-flop break points. The knock-in was carried out using gene replacement strategy as described previously (4, 5). The two gene units, *tet0/xyl* and *gfp*, which were suitable for recombination into the desired flip-flop breakpoint regions of *S. aureus* chromosome, were cloned into pKOR1 (4) to generate plasmids pKOR1-tetO/xyl and pKOR1-gfp, respectively. For constructing pKRO1-tetO/xyl, three PCR fragments, namely, the *tet0/xyl* fragment from pWH353 (6) together with 821- and 1,500-bp-long fragments located at the right flip-flop breakpoint region on the Mu50Ω1 genome (PCR amplified from nucleotide positions 87,5398–87,6218 for the former and 87,3046–87,4545 for the latter; Fig. 5*A*), were cloned into pKOR1 using restriction enzyme *EcoRI* and ligation to connect the 821-bp fragment to *tetO/xyl*, whereas *SmaI* restriction and ligation connected *tetO/xyl* to the 1,500-bp fragment. Both of these fragments carried attB1 and attB2 recombination sites, which were also available on pKOR1 (4). The resulting plasmid, designated as pKOR1-tetO/xyl, was introduced into type A genome Mu50Ω1 cells, and the gene replacement procedure was carried out as described previously (5). Briefly, the overnight cultures of plasmid-carrying clones were plated at 43 °C to select single cross-over mutants that carried pKRO1-tetO/xyl on the Mu50Ω1 chromosome. The single cross-over mutants were then cultured in drug-free broth to facilitate plasmid excision and subjected to anhydrotetracycline induction, whereby only non–plasmid-carrying mutants could survive. To check for successful introduction of the *tetO/xyl* with the correct "forward" direction, resulting mutants were checked for the target sequences via sequencing. Resulting mutant Mu50Ω1-tet0/xyl carries *tetO/xyl* on its chromosome with the fragment located just upstream of the right flip-flop breakpoint region in a forward direction (Fig. 5*B*, I). By using the same strategy, pKOR1-gfp was introduced into Mu50Ω1-tet0/xyl cells and the *gfp* gene was knocked-in into Mu50Ω1-tet0/xyl chromosome at the left flip-flop breakpoint region in a reversed direction to generate Mu50Ω1-tet0/xyl-gfp (Fig. 5*B*, I). It was expected that once the flip-flop occurs, the *gfp* fragment will be relocated just downstream of the *tet0/xyl* promoter in a forward direction, allowing GFP protein production when the *tet0/xyl* promoter was induced by tetracycline (Fig. 5*B*, II). The expression of GFP was observed under fluorescent microscopy.

Theoretical Calculation of the Flip-Flop Probabilities Between Mu50Ω1 and Mu50Ω2. ***I. Introduction.*** To determine the flip-flop probabilities between Mu50Ω1 and Mu50Ω2 from the experimental data, we will develop a theoretical model of the bacteria growth in this report.

We denote two genotypes of bacteria as type A (majority cell populations of Mu50Ω1) and type B (majority cell populations of Mu50Ω2), and their frequencies as y_s and y_n. There are two stable colony types, Mu50Ω1 (small colony variant) and Mu50Ω2 (normal colony variant) as described in the main text. These two are certain admixtures of bacteria with type A and B genomes, with the former being mainly composed of type A bacteria (admixture of y_n is about 0.1–0.3%) and the latter being mainly

composed of type B bacteria (admixture of y_s is about 1–10%). An important experimental finding is that the frequency ratio, y_n/y_s, is constant under the experimental condition, where a portion of the liquid culture is daily transferred to a different liquid medium to passage for 10 d. This feature brings a remarkable consequence that the flip-flop probabilities between type A and type B in Mu50Ω1 and Mu50Ω2 are different. We will prove this fact in the next section with a simple case of exponential growth phase. In later sections, we will fix the values of flip-flop probabilities using a more sophisticated model.

II. Different values of flip-flip probabilities in Mu50Ω1 and Mu50Ω2. In this section, we will analyze the experimental data by focusing on the exponential growth phase of the bacteria. Through the whole exponential phase, the experiment data show that the y_n/y_s value in Mu50Ω1 keeps constant at about 0.001–0.003, whereas the value of y_n/y_s in Mu50Ω2 is about 90.0–99.0. We will demonstrate below that it cannot be possible to keep such two values constant if the flip-flop probability is same in both Mu50Ω1 and Mu50Ω2.

Denoting a_s and a_n for the growth rates of type A and type B bacteria, we can express the growth of y_s and y_n in Mu50Ω1 or in Mu50Ω2 as follows:

$$\frac{dy_s}{dt} = \alpha_s(1 - w_{s\to n})y_s + \alpha_n w_{n\to s} y_n, \qquad \textbf{[S1]}$$

$$\frac{dy_n}{dt} = \alpha_n(1 - w_{n\to s})y_n + \alpha_s w_{s\to n} y_s, \qquad \textbf{[S2]}$$

where the symbols $w_{s\to n}$ and $w_{n\to s}$ stand for the flip-flop probabilities per one doubling of bacteria with type A or type B genome. We are concerned with the ratio y_n/y_s, and define the quantity as

$$r(t) = y_n(t)/y_s(t). \qquad \textbf{[S3]}$$

By calculating the derivative using Eqs. **S1** and **S2**, we obtain

$$\frac{dr(t)}{dt} = -r(t)^2\alpha_n w_{n\to s} - r(t)[a_s(1 - w_{s\to n}) - \alpha_n(1 - w_{n\to s})] + \alpha_s w_{s\to n}. \qquad \textbf{[S4]}$$

This is an inverse parabola function of $r(t)$, which has two real intercept points $R_1 > 0$ and $R_2 < 0$ of $r(t)$-axis. By definition, $r(t)$ is positive definite; therefore, if the initial value of $r(t)$ at $t = 0$ is $0 \le r(0) < R_1$, the derivative of $r(t)$ is positive for nonzero flip-flop probability. This means that the $r(t)$ value increases up to the value of R_1, where it should stop rising because the derivative is zero. If the initial value of $r(t)$ at $t = 0$ is larger than R_1, the derivative of $r(t)$ is negative and decreases to the point R_1, where the decrement will stop because the derivative is zero. Therefore, irrespective of the initial value, the ratio y_n/y_s always approaches R_1, which is a unique attractor of the dynamic system.

Experimentally, there occur two stable values of the ratio y_n/y_s corresponding to Mu50Ω1 and Mu50Ω2. This fact contradicts the above theoretical considerations. This contradiction between the theory and experimental data, however, can be resolved if some of the values of a_s, a_n, $w_{s\to n}$, and $w_{n\to s}$ are not constant. That means some parameter values in Mu50Ω1 and in Mu50Ω2 should be different. Theoretically, it is not easy to determine which parameters are responsible for this phenomenon. We assume here that the growth rate parameters, a_s and a_n, are constant and seek for a change in either $w_{s\to n}$ or $w_{n\to s}$. To analyze and extract the parameter values from the experimental data, we need to generalize Eqs. **S1** and **S2** to a form that includes bacterial density and lysis effects.

III. Generation of coupled Bernoulli equations for fitting to data. The growth curve of bacteria can be fitted by several theoretical curves, among which we adopt the one called the Bernoulli equation (7). Denoting y as the frequency of bacteria, the form is written as

$$\frac{dy}{dt} = \alpha y\left[1 - (y/K)^\theta\right], \qquad \textbf{[S5]}$$

which contains three parameters: α, K, and θ. For the bacteria growth, α is the growth rate and K is the saturation value, which is also called "carrying capacity." The parameter θ controls the way in which frequency approaches the asymptotic value K. If we put θ = 1, the Bernoulli equation reduces to the logistic equation. This nonlinear equation can be integrated analytically to get the expression

$$y = \frac{K}{[1 + C\exp(-\alpha\theta t)]^{1/\theta}}, \qquad \textbf{[S6]}$$

where C is an integration constant. The next task is to fix the coupled Bernoulli equations for the competitive growth of the bacteria y_s and y_n in the stirred liquid medium starting from the solution of a colony of Mu50Ω1 or Mu50Ω2. We follow a standard way to get the Lotka–Volterra equation from the logistic equation, as given by Vandermeer and Goldberg (8). It represents a competitive growth of the two species, which share a similar niche in addition to the flip-flop transitions. The resulting equations are written as

$$\frac{dy_s}{dt} = \alpha_s F_s y_s - \alpha_s f_s w_{s\to n} y_s + \alpha_n f_n w_{n\to s} y_n, \qquad \textbf{[S7]}$$

$$\frac{dy_n}{dt} = \alpha_n F_n y_n - \alpha_n f_n w_{n\to s} y_n + \alpha_s f_s w_{s\to n} y_s, \qquad \textbf{[S8]}$$

where

$$F_s = 1 - \left(\frac{y_s + c_n y_n}{K_s}\right)^\theta, \qquad \textbf{[S9]}$$

$$F_n = 1 - \left(\frac{y_n + c_s y_s}{K_n}\right)^\theta, \qquad \textbf{[S10]}$$

and

$$f_s = F_s \ \text{(if } F_s \text{ is positive)}, \qquad \textbf{[S11]}$$

$$= 0 \ \text{(if } F_s \text{ is negative)}, \qquad \textbf{[S12]}$$

$$f_n = F_n \ \text{(if } F_n \text{ is positive)}, \qquad \textbf{[S13]}$$

$$= 0 \ \text{(if } F_n \text{ is negative)}. \qquad \textbf{[S14]}$$

In these equations, we use the following symbols (s and S for small colony Mu50Ω and n and N for normal colony Mu50Ω):

- y_s: Amount of small colony-forming bacteria (S-bacteria, which have type A genome)
- y_n: Amount of normal colony-forming bacteria (N-bacteria, which have type B genome)
- α_s: Time constant for S-bacteria
- α_n: Time constant for N-bacteria
- $w_{s\to n}$: Transition probability from S-bacteria to N-bacteria
- $w_{n\to s}$: Transition probability from N-bacteria to S-bacteria
- K_s: Asymptotic value of the evolution of S-bacteria
- K_n: Asymptotic value of the evolution of N-bacteria
- c_n: Effect of N-bacteria on the evolution of S-bacteria

- c_s: Effect of S-bacteria on the evolution of N-bacteria
- θ: Exponent that controls the way of approach to the asymptotic value

It should be noted that the quantity $K_s(K_n)$ in Eqs. **S9** and **S10** is defined as an asymptotic value of the total number of S-bacteria (N-bacteria). The generalization for including the different values of K_s and K_n, together with the introduction of c_s and c_n, is the basis of this generalized Lotka–Volterra model (coupled Bernoulli model) for calculating the competition between two similar species requiring a similar "niche."

What is unique in our present study is that in addition to these terms, there are also terms of the transition to and from between two species ($y_s \Leftrightarrow y_n$) represented by the second and third terms in the right hand side (r.h.s) of Eqs. **S7** and **S8**. Through these flip-flop terms, it is possible that two species compete with each other even if we start from purely one kind of species at the initial time. These transition terms can cause a modification of the original Lotka–Volterra equation in such a way that complete exclusion of one species is avoided. A caution should be given here about the difference in the quantities between F_s, F_n and f_s, f_n. The former quantities express the density dependency, which can take both positive and negative values. The latter quantities, on the other hand, cannot take a negative value because they are used for the flip-flop transitions, which can take place only at the time of doubling and not at the time when the number of bacteria decreases.

IV. Introduction of bacteria degradation factor into the equation. In the Bernoulli equation, the number of bacteria approaches to a saturation after a long time, as is clear in Eq. **S6**. This is true for some time range, but when a batch job is treated for a longer time range, the total number of bacteria in this system begins to decrease. (Attention should be paid to the fact that the simple death of some bacteria is always compensated for by the birth of new bacteria, which does not lead to a decrease in the total number of living bacteria.) To include this effect, we introduce phenomenologically a damping factor $\exp(-\beta t^2)$, which stands for the decrease in the total number of bacteria. To generate a new equation that includes this degradation effect, we impose that the solution of Eq. **S6** should be changed to

$$y = \frac{K\ \exp(-\beta t^2)}{\left[1 + C\ \exp(-\alpha\theta t)^{1/\theta}\right.}. \qquad \textbf{[S15]}$$

This form is adopted purely phenomenologically. We then seek for the differential equation whose solution obeys Eq. **S15**. By differentiating Eq. **S15** and using original Eq. **S15**, we obtain

$$\frac{dy}{dt} = y\alpha'\left[1 - \left(\frac{y}{K'(t)}\right)^{\theta}\right], \qquad \textbf{[S16]}$$

where the newly defined growth rate α' is defined as

$$\alpha'(t) = \alpha - 2\beta t, \qquad \textbf{[S17]}$$

and the asymptotic value of bacteria $K'(t)$ is given by

$$K'(t) = K\left(1 - \frac{2\beta t}{\alpha}\right)^{1/\theta}\exp(-\beta t^2). \qquad \textbf{[S18]}$$

These are used in the following calculations for the positive value of $\alpha'(t)$. It is easy to ascertain that Eq. **S16** approaches Eq. **S5** as β approaches to zero, because in this limit, $K'(t)$ approaches to K and α' approaches to α. For simplicity, we assume that the damping factor $\exp(-\beta t^2)$ is common to both y_s and y_n.

The next task is to generalize the coupled Bernoulli Eqs. **S7** and **S8** after the effect of this degradation is included. For this purpose, the procedure described in the previous section is followed, where the effect of degradation is now incorporated. We will skip to give the complete description of this generalized coupled equation, but the essential change is to replace α and K in Eqs. **S7** and **S8** by $a(t)'$ and $K'(t)$ and no other change. The degradation effect is not large at all as the following analysis will show, only affecting the behavior after 2 d or so.

V. Numerical fitting to the experimental data and discussion. The main purpose of the data analysis is to obtain the values of parameters $w_{s\to n}$ and $w_{n\to s}$. However, the values of parameters a_s, a_n, K_s, K_n, c_s, C_n, θ, and β should also be fixed. Among them, the growth rate parameters a_s and a_n are fixed as the following values by the seven independent experiments in which the doubling times of bacteria in the exponential growing phase are measured:

- $\alpha_s = 0.01787\ \text{min}^{-1}$: Corresponding to doubling time 38.79 min of Mu50Ω1
- $\alpha_n = 0.02221\ \text{min}^{-1}$: Corresponding to doubling time 31.21 min of Mu50Ω2

At this point, we are left with eight unknown parameters, and these are fixed by fitting to the four kinds of bacteria data in the stirred BHI solution. Two curves shown in Fig. 7 are the bacterial growth curves as a function of time. A portion of fresh bacterial cultures started from a single colony of a small colony (from Mu50Ω1) or a normal colony (from Mu50Ω2) is applied to measure growth curves. For time $t = 0$, the bacterial concentration is adjusted to about 1,000 cells and bacterial cultures are then sampled at indicated times to spread on drug-free BHI agar plates to count bacterial colony. For each sample, small and normal colonies are counted and plotted to generate the growth curves up to 4,500 min (3.125 d).

The theoretical model developed in previous two sections is used for the fitting. In the calculation of the coupled Bernoulli equation with the bacteria degradation factor by the Runge–Kutta method, the best-fit values of the parameters are determined as follows:

- $K_s = 3.60 \times 10^9$
- $K_n = 1.80 \times 10^9$
- $c_n = 1.97$
- $c_s = 0.50$
- $\theta = 0.50$
- $\beta = 1.90 \times 10^{-8}\ \text{min}^{-1}$

We obtain the flip-flop probabilities as follows:

$$w_{s\to n} = 3.0\times10^{-5}(\text{for both Mu50Ω1 and Mu50Ω2}), \qquad \textbf{[S19]}$$

$$w_{n\to s} = 2.5\times10^{-1}(\text{for Mu50Ω1}), \qquad \textbf{[S20]}$$

$$w_{n\to s} = 2.0\times10^{-2}(\text{for Mu50Ω2}). \qquad \textbf{[S21]}$$

We should offer some remarks on why so many parameters can be fixed. The values of K_s and K_n are obtained directly from the asymptotic values of the growth curves. The values of c_s and c_n can be estimated because they should be about 2.0 and 0.5, respectively. This is because they are related to the values of K_s and K_n, where the former is twice as large as the latter, as given above. The values of θ and β can be fixed by the behavior of approaching to saturations and the rate of the decrease in saturated values, respectively.

In Fig. 7, we show the calculated results for the change in bacterial number as a function of time together with experimental data. Fig. 7 (*Left*) shows the result for the initial condition starting from a small colony (Mu50Ω1). Fig. 7 (*Right*) shows the result for the initial condition starting from a normal colony (Mu50Ω2). In these figures, the solid curve and blue circle correspond to calculated and experimental numbers of S-bacteria,

and the dotted curve and red diamond correspond to calculated and experimental numbers of N-bacteria. We obtain the following two important results: (*i*) asymmetry of the flip-flop probability between $w_{s\to n}$ and $w_{n\to s}$ and (*ii*) asymmetry of the flip-flop probability from N to S between Mu50Ω1 and Mu50Ω2. From Fig. 7, we can certify that the value of $w_{n\to s}$ does change according to the environmental condition, whether it is in Mu50Ω1 or Mu50Ω2.

Although an asymmetrical flip-flop probability in the cell populations of Mu50Ω1 and Mu50Ω2 is clear, caution should be paid with respect to the determination of $w_{s\to n}$ and $w_{n\to s}$. What can be determined is only a difference in the transition between N → S and S → N, and it is impossible to know the absolute rates because there is no way to isolate any colony that consists of pure cells with genotype A or B because of the constant occurrence of the flip-flop inversion between the two type genomes. In calculations, we fixed the value $w_{s\to n}$ as 3.0×10^{-5}, based on the fact that growth of S-bacteria produces admixture of N-bacteria of only about 1/300 even though the N-bacteria have a doubling time about 20% shorter than the S bacteria. The absolute value, however, is a kind of conjecture and cannot be determined precisely. We assume this value is applicable to both Mu50Ω1 and Mu50Ω2 when looking for the value of $w_{n\to s}$. It should be noted that a few orders of change of the value of $w_{s\to n}$ in Mu50Ω2 cause essentially no change in the values of $w_{n\to s}$. The main conclusion on the asymmetry between $w_{s\to n}$ and $w_{n\to s}$, and the asymmetry of $w_{n\to s}$ in Mu50Ω1 and in Mu50Ω2, does not depend on the assumed $w_{s\to n}$ value of 3.0×10^{-5}.

We found that the flip-flop probability (defined as what portion is rearranged per single doubling of bacteria) is quite asymmetrical; that is, the transition from S to N is less than that of N to S by several orders of magnitude. However, the more fascinating observation is that the flip-flop probability from N to S takes two different values in Mu50Ω1 and Mu50Ω2 (i.e., the value in the former is larger than in the latter by a single order of magnitude). This is what we discussed in Section II (Different values of flip-flip probabilities in Mu50Ω1 and Mu50Ω2), and it is a manifestation of the conclusion that one common value of flip-flop probability cannot explain the existence of two stable compositions seen in Mu50Ω1 and Mu50Ω2.

1. Cui L, Neoh HM, Shoji M, Hiramatsu K (2009) Contribution of *vraSR* and *graSR* point mutations to vancomycin resistance in vancomycin-intermediate Staphylococcus aureus. *Antimicrob Agents Chemother* 53:1231–1234.
2. Hiramatsu K, et al. (1997) Methicillin-resistant Staphylococcus aureus clinical strain with reduced vancomycin susceptibility. *J Antimicrob Chemother* 40:135–136.
3. Cui L, Murakami H, Kuwahara-Arai K, Hanaki H, Hiramatsu K (2000) Contribution of a thickened cell wall and its glutamine nonamidated component to the vancomycin resistance expressed *by Staphylococcus aureus* Mu50. *Antimicrob Agents Chemother* 44:2276–2285.
4. Bae T, Schneewind O (2006) Allelic replacement in Staphylococcus aureus with inducible counter-selection. *Plasmid* 55(1):58–63.
5. Neoh HM, et al. (2008) Mutated response regulator graR is responsible for phenotypic conversion of Staphylococcus aureus from heterogeneous vancomycin-intermediate resistance to vancomycin-intermediate resistance. *Antimicrob Agents Chemother* 52: 45–53.
6. Geissendörfer M, Hillen W (1990) Regulated expression of heterologous genes in Bacillus subtilis using the Tn10 encoded tet regulatory elements. *Appl Microbiol Biotechnol* 33:657–663.
7. Thieme HR (2003) *Classical Models of Density-Dependent Population Growth for Single Species* (Princeton Univ Press, Princeton).
8. Vandermeer JH, Goldberg DE (2003) *Competition and a Little Bit of Mutualism* (Princeton Univ Press, Princeton).

Table S1. Antibiotic susceptibility profiles of *S. aureus* strains used in this study*

		MICs for Mu50Ω1		MICs for Mu50Ω2	
Antibiotics	E-test code	24 h	48 h	24 h	48 h
Ampicillin	AM	1 (8)†	1 (8)†	4	4
Ampicillin/sulbactam	AB	2 (32)†	2 (32)†	10	12
Methicillin	ME	>256†	>256†	>256	>256
Oxacillin	OX	8 (128)†	8 (128)†	>256	>256
Imipenem	IP	0.38 (32)†	0.38 (32)†	32	32
Cephalothin	CE	0.25 (128)	0.38 (128)†	>256	>256
Ceftizoxime	CZ	0.38 (256)	0.5 (256)†	>256	>256
Cefoxitin	FX	32 (256)†	32 (256)†	>256	>256
Ceftriaxone	TX	3 (256)†	4 (256)†	>256	>256
Vancomycin	VA	0.75	1	1	1
Teicoplanin	TP	0.5	1	1	1
Fosfomycin	FM	>1,024	>1,024	>1,024	>1,024
Bacitracin	BA	12	24	12	16
Erythromycin	EM	>256	>256	>256	>256
Clarithromycin	CH	>256	>256	>256	>256
Azithromycin	AZ	>256	>256	>256	>256
Tetracycline	TC	32	48	24	32
Doxycycline	DC	8	>256	8	>256
Minocycline	MC	10	24	8	12
Chloramphenicol	CL	4	4	4	4
Gentamicin	GM	64	64	96	96
Quinupristin/dalfopristin	QDA	0.5	1	0.5	0.5
Clindamycin	CM	>256	>256	>256	>256
Levofloxacin	LE	>32	>32	>32	>32
Sparfloxacin	SO	>32	>32	>32	>32
Ciprofloxacin	CI	>32	>32	>32	>32
Colistin	CO	64	48	128	256
Daptomycin	DPC	1	1	1	1
Linezolid	LZ	0.5	0.5	0.5	0.5

*MICs were determined by E-test on a Mueller-Hinton (MH) agar plate with a 24-h incubation at 37 °C. MICs for a 48-h incubation were also recorded because Mu50Ω1 grows slowly.

†Heterogeneous resistance with about 1 in 10^3 to 1 in 10^4 cells having high MIC values, as shown in parentheses, when confirmed by the agar dilution method.

Table S2. Transcriptional profile of genes up-regulated in Mu50Ω2 vs. Mu50Ω1

Gene information			
ORF	Name	Product	Ratio (Mu50Ω2/Mu50Ω1)
Cell envelope and cellular processes (category I)			
SA0295	—	Hypothetical protein, similar to outer membrane protein precursor	2.21
SA0758	—	Hypothetical protein, similar to thioredoxin	2.11
SA0769	—	ABC transporter ATP-binding protein homolog	2.33
SA1042	pyrP	Uracil permease	3.05
SA1341	—	Similar to export protein SpcT protein	2.10
SA1381	pbp3	Penicillin-binding protein 3	1.97
SA1475	—	Hypothetical protein, similar to cell shape determinant mreC	2.46
SA1852	vga	Hypothetical ABC transporter ATP-binding protein	2.68
SA1880	kdpB	Probable potassium-transporting ATPase B chain	2.02
SA1893	—	Lipoprotein precursor	1.97
SA1902	murA	UDP-*N*-acetylglucosamine-1-carboxyvinyl transferase-1	2.84
SA2020	—	Hypothetical protein, similar to ABC transporter (ATP-binding protein)	2.19
SA2021	—	Hypothetical protein, similar to ABC transporter (ATP-binding protein)	2.19
SA2053	—	Glucose uptake protein homolog	2.42
SA2057	fmhB	FmhB protein	2.74
SA2079	—	Hypothetical protein, similar to ferrichrome ABC transporter fhuD precursor	2.11
SA2100	—	Hypothetical protein, similar to autolysin E	2.79
SA2112	—	Hypothetical protein, similar to sodium-dependent transporter	2.28
SA2114	glvC	PTS system, arbutin-like IIBC component	2.77
SA2117	—	Hypothetical protein, similar to Na^+/H^+ antiporter, putative	2.07
SA2135	—	Hypothetical protein, similar to sodium/glutamate symporter	2.45
SA2137	—	Hypothetical protein, similar to divalent cation transport	2.19
SA2142	—	Hypothetical protein, similar to multidrug resistance protein	3.18
SA2152	—	Hypothetical protein, similar to two component histidine kinase sensor	2.41
SA2166	—	Hypothetical protein, similar to cationic transporter	2.02
SA2191	—	Hypothetical protein, similar to NirC	2.38
SA2228	—	Hypothetical protein, similar to NA^+/H^+ exchanger	1.96
SA2241	—	Hypothetical protein, similar to chloramphenicol resistance protein	1.95
SA2261	—	Hypothetical protein, similar to efflux pump	2.41
SA2293	gntP	Gluconate permease	1.96
Intermediary metabolism (category II)			
SA0511	—	Hypothetical protein, similar to UDP-glucose 4-epimerase related protein	2.06
SA0654	fruB	Fructose-1-phosphate kinase	2.11
SA0685	nrdI	NrdI protein involved in ribonucleotide reductase function	2.31
SA0756	—	Hypothetical protein, similar to 3-dehydroquinate dehydratase	3.25
SA0776	—	Aminotransferase NifS homolog	1.98
SA0785	lipA	Lipoic acid synthetase	2.12
SA1043	pyrB	Aspartate transcarbamoylase chain A	1.96
SA1858	ilvD	Dihydroxy-acid dehydratase	2.29
SA1859	ilvB	Acetolactate synthase large subunit	2.12
SA1874	alr	Alanine racemase	2.57
SA1901	—	(3R)-hydroxymyristoyl-(acyl carrier protein) dehydratase	2.44
SA1940	deoD	Purine nucleoside phosphorylase	2.15
SA2001	—	Hypothetical protein, similar to oxidoreductase, aldo/keto-reductase family	1.96
SA2068	moeA	Molybdopterin biosynthesis protein moeA	2.17
SA2070	moaB	Molybdopterin precursor biosynthesis moaB	2.09
SA2078	—	Similar to inosine-adenosine-guanosine-nucleoside hydrolase	2.25
SA2080	—	Hypothetical protein, similar to butyryl-CoA dehydrogenase	3.02
SA2087	ureG	Urease accessory protein UreG	2.64
SA2088	ureD	Urease accessory protein UreD	1.95
SA2095	—	Hypothetical protein, similar to D-octopine dehydrogenase	2.00
SA2111	—	Hypothetical protein, similar to phosphoglycolate phosphatase	2.71
SA2127	—	Hypothetical protein, similar to ribose 5-phosphate isomerase	2.39
SA2140	—	Hypothetical protein, similar to esterase	1.97
SA2204	—	Phosphoglycerate mutase, pgm homolog	1.98
SA2211	—	Hypothetical protein, similar to 6-carboxyhexanoate–CoA ligase	1.98
SA2231	—	Hypothetical protein, similar to glucose epimerase	1.97
SA2232	—	Hypothetical protein, similar to 2-dehydropantoate-2-reductase	2.13
SA2248	—	Hypothetical protein, similar to glutamate synthase (ferredoxin)	1.98
Information pathways (category III)			

Table S2. Cont.

Gene information			
ORF	Name	Product	Ratio (Mu50Ω2/Mu50Ω1)
SA0348	—	Hypothetical protein, similar to transcription terminator	1.96
SA0653	—	Hypothetical protein, similar to transcription repressor of fructose operon	2.18
SA1041	pyrR	Pyrimidine operon repressor chainA	2.22
SA1093	—	DNA topoisomerase I topA homolog	2.18
SA1290	—	Hypothetical protein, similar to poly(A) polymerase	2.05
SA1847	scrR	Sucrose operon repressor	2.12
SA1854	—	Hypothetical protein, similar to O-sialoglycoprotein endopeptidase	2.23
SA1855	—	Hypothetical protein, similar to ribosomal-protein-alanine *N*-acetyltransferase	2.28
SA1856	—	Hypothetical protein, similar to glycoprotein endopeptidase	2.40
SA2018	truA	tRNA pseudouridine synthase A	2.07
SA2038	rpsQ	30S ribosomal protein S17	10.86
SA2108	—	Hypothetical protein, similar to transcription regulator, RpiR family	2.02
SA2151	—	Hypothetical protein, similar to two component response regulator	2.30
SA2174	sarZ	Hypothetical protein, similar to transcriptional regulator	2.19
SA2287	sarH2	Staphylococcal accessory regulator A homolog	2.24
SAS093	rpmH	50S ribosomal protein L34	2.52
Other functions (category IV)			
SA0393	set15	Exotoxin 15 (pathogenicity island SaPIn2)	2.24
SA0745	—	Hypothetical protein, similar to extracellular matrix and plasma binding	1.97
SA0759	—	Hypothetical protein, similar to arsenate reductase	2.34
SA1835	int	Hypothetical protein, similar to integrase (pathogenicity island SaPIn1)	2.20
SA1969	—	Hypothetical protein, similar to ATP-binding Mrp-like protein	2.14
SAS077	—	Hypothetical protein, similar to transposase for IS232	1.97
SA2175	—	Hypothetical protein, similar to small heat shock protein	1.97
Similar to unknown proteins (category V)			
SA0037	—	Conserved hypothetical protein	2.82
SA0100	—	Conserved hypothetical protein	2.55
SA0467	—	Conserved hypothetical protein	2.20
SA0601	—	Conserved hypothetical protein	2.12
SA0750	—	Conserved hypothetical protein	2.20
SA0770	—	Conserved hypothetical protein	2.88
SA0782	—	conserved hypothetical protein	3.05
SA1840	—	Conserved hypothetical protein	2.00
SA1849	—	Conserved hypothetical protein	2.85
SA1850	—	Conserved hypothetical protein	2.19
SA1857	—	Conserved hypothetical protein	2.17
SA1873	—	Conserved hypothetical protein	2.00
SA1890	—	Conserved hypothetical protein	3.82
SA1900	—	Conserved hypothetical protein	2.35
SA1903	—	Conserved hypothetical protein	1.98
SA1918	—	Conserved hypothetical protein	2.21
SA1928	—	Hypothetical protein	2.86
SA1932	—	Similar to hypothetical protein T13D8.31, *Arabidopsis thaliana*	2.51
SA1942	—	Conserved hypothetical protein	3.06
SA1957	—	Conserved hypothetical protein	2.09
SA1990	—	Conserved hypothetical protein	3.27
SA2005	—	Conserved hypothetical protein	2.24
SA2019	—	Conserved hypothetical protein	2.25
SA2054	—	Conserved hypothetical protein	2.75
SA2106	—	Hypothetical protein, similar to protein of pXO2-46	2.31
SA2130	—	Conserved hypothetical protein	2.43
SA2138	—	Conserved hypothetical protein	1.98
SA2143	—	Conserved hypothetical protein	5.96
SA2146	tcaA	TcaA protein	2.00
SA2150	—	Conserved hypothetical protein	1.99
SA2153	—	Conserved hypothetical protein	2.18
SA2163	—	Hypothetical protein	2.20
SA2193	—	Conserved hypothetical protein	2.20
SA2197	—	Conserved hypothetical protein	2.68
SA2205	—	Conserved hypothetical protein	2.06
SA2225	—	Conserved hypothetical protein	2.04

Table S2. Cont.

Gene information			
ORF	Name	Product	Ratio (Mu50Ω2/Mu50Ω1)
SA2238	—	Conserved hypothetical protein	1.97
SA2256	—	Conserved hypothetical protein	1.96
SA2284	—	Hypothetical protein, similar to accumulation-associated protein	8.43
SA2285	—	Hypothetical protein, similar to accumulation-associated protein	10.52
No similarity (category VI)			
SA1641	—	Hypothetical protein (pathogenicity island SaPIn3)	2.34
SA1834	—	Hypothetical protein (pathogenicity island SaPIn1)	2.90
SAS068	—	Hypothetical protein	2.16
SA1889	—	Hypothetical protein	2.80
SA1933	—	Hypothetical protein	2.53
SA1943	—	Hypothetical protein	2.54
SA2049	—	Hypothetical protein	2.50
SA2059	—	Hypothetical protein	2.06
SA2076	—	Hypothetical protein	2.34
SA2107	—	Hypothetical protein	2.05
SA2113	—	Hypothetical protein	2.51
SA2113	—	Hypothetical protein	2.51
SA2116	—	Hypothetical protein	2.91
SA2118	—	Hypothetical protein	2.06
SA2126	—	Hypothetical protein	1.97
SAS086	—	Hypothetical protein	2.02
SA2157	—	Hypothetical protein	2.33
SA2198	—	Hypothetical protein	2.40
SA2218	—	Hypothetical protein	2.07
SA2221	—	Hypothetical protein	2.27
SA2224	—	Hypothetical protein	2.59
SA2267	—	Hypothetical protein	2.09
SAV0406	—	Hypothetical protein	2.00
SAV0791	—	Hypothetical protein	2.08
SAV0802	—	Hypothetical protein	2.36

ABC, ATP binding cassette; PTS, phosphotransferase system; IIBC, type B and C component of type II PTS.

Table S3. Transcriptional profile of genes down-regulated in Mu50Ω2 vs. Mu50Ω1

Gene information			
ORF	Name	Product	Ratio (Mu50Ω2/Mu50Ω1)
Cell envelope and cellular processes (category I)			
SA0214	uhpT	Hexose phosphate transport protein	0.18
SA0217	—	Hypothetical protein, similar to periplasmic-iron-binding protein BitC	0.47
SA0265	lytM	Peptidoglycan hydrolase	0.51
SA0272	—	Hypothetical protein, similar to transmembrane protein Tmp7	0.33
SA0293	—	Hypothetical protein, similar to formate transporter NirC	0.44
SA0297	—	Hypothetical protein, similar to ABC transporter ATP-binding protein	0.31
SA0456	spoVG	Stage V sporulation protein G homolog	0.53
SA0531	proP	Proline/betaine transporter homolog	0.47
SA0600	—	Hypothetical protein, similar to pyrimidine nucleoside transporter	0.53
SA0640	—	Similar to ABC transporter required for expression of cytochrome bd	0.44
SA0682	—	Hypothetical protein, similar to di-tripeptide ABC transporter	0.52
SA0808	mnhF	Na^+/H^+ antiporter subunit	0.50
SA0847	oppD	Oligopeptide transport system ATP-binding protein OppD homolog	0.43
SA0868	—	Na^+/H^+ antiporter homolog	0.51
SA0891	—	Hypothetical protein, similar to ferrichrome ABC transporter	0.49
SA0951	potB	Spermidine/putrescine ABC transporter homolog	0.52
SA1023	ftsL	Cell division protein	0.46
SA1025	mraY	Phospho-*N*-muramic acid-pentapeptide translocase	0.36
SA1026	murD	UDP-*N*-acetylmuramoylalanine-D-glutamate ligase	0.50
SA1028	ftsA	Cell division protein	0.40
SA1269	—	Blt-like protein	0.51
SA1270	—	Hypothetical protein, similar to amino acid permease	0.42
SA2167	scrA	PTS system, sucrose-specific IIBC component	0.42
Intermediary metabolism (category II)			
SA0118	—	Hypothetical protein, similar to various aldolase	0.55
SA0131	pnp	Purine nucleoside phosphorylase	0.43
SA0176	—	Hypothetical protein, similar to *N*-acetylglutamate-5-phosphotransferase	0.47
SA0219	pflA	Formate acetyltransferase activating enzyme	0.29
SA0225	—	Hypothetical protein, similar to glutaryl-CoA dehydrogenase	0.41
SA0232	lctE	L-lactate dehydrogenase	0.41
SA0431	gltD	NADH-glutamate synthase small subunit	0.53
SA0562	adh1	Alcohol dehydrogenase I	0.33
SA0818	rocD	Ornithine aminotransferase	0.43
SA0822	argG	Argininosuccinate synthase	0.53
SA0896	mend	Menaquinone biosynthesis protein	0.54
SA0916	—	Hypothetical protein, similar to phosphoribosylaminoimidazole carboxylase PurE	0.52
SA1075	hmrB	HmrB protein	0.44
SA1271	—	Threonine deaminase IlvA homolog	0.43
SA1272	—	Alanine dehydrogenase	0.40
SA1338	mala	α-D-1,4-glucosidase	0.50
SA1584	—	Lysophospholipase homolog	0.48
SA1585	—	Proline dehydrogenase homolog	0.55
SA2294	gntK	Gluconokinase	0.49
SA2464	hisI	Histidine biosynthesis bifunctional protein HisIE	0.46
SA2466	—	Similar to phosphoribosylformimino-5-aminoimidazole carboxamide ribotide isomerase	0.44
SA2467	hisH	Amidotransferase hisH	0.55
SA2470	—	Hypothetical protein, similar to histidinol dehydrogenase	0.50
SA2471	hisG	ATP phosphoribosyltransferase	0.54
SA2472	—	Hypothetical protein, similar to ATP phosphoribosyltransferase regulatory subunit	0.55
Information pathways (category III)			
SA0815	—	Peptidyl-prolyl cis-trans isomerase homolog	0.51
SA0836	—	Hypothetical protein, similar to transcription regulator LysR family	0.52
SA0897	—	Hypothetical protein, similar to prolyl aminopeptidase (EC 3.4.11.5)	0.45
SA1063	—	Protein kinase	0.53
SA1067	rpmB	50S ribosomal protein L28	0.41
SA1098	codY	Transcription pleiotropic repressor codY	0.53
SA1139	glpP	Glycerol uptake operon antiterminator regulatory protein	0.48
SA1339	malR	Maltose operon transcriptional repressor	0.55
SA1414	rpsT	30S ribosomal protein S20 (BS20)	0.52
SA2295	gntR	Gluconate operon transcriptional repressor	0.45

Table S3. Cont.

Gene information			
ORF	Name	Product	Ratio (Mu50Ω2/Mu50Ω1)
Other functions (category IV)			
SA0132	—	Hypothetical protein, similar to tetracycline resistance protein	0.52
SA0144	capA	Capsular polysaccharide synthesis enzyme Cap5A	0.34
SA0145	capB	Capsular polysaccharide synthesis enzyme Cap5B	0.24
SA0146	capC	Capsular polysaccharide synthesis enzyme Cap8C	0.40
SA0147	capD	Capsular polysaccharide synthesis enzyme Cap5D	0.30
SA0148	cape	Capsular polysaccharide synthesis enzyme Cap8E	0.36
SA0149	capF	Capsular polysaccharide synthesis enzyme Cap5F	0.34
SA0150	capG	Capsular polysaccharide synthesis enzyme Cap5G	0.33
SA0151	capH	Capsular polysaccharide synthesis enzyme O-acetyl transferase Cap5H	0.46
SA0153	capJ	Capsular polysaccharide synthesis enzyme Cap5J	0.43
SA0154	capK	Capsular polysaccharide synthesis enzyme Cap5K	0.51
SA0155	capL	Capsular polysaccharide synthesis enzyme Cap5L	0.26
SA0156	capM	Capsular polysaccharide synthesis enzyme Cap5M	0.49
SA0158	capo	Capsular polysaccharide synthesis enzyme Cap8O	0.43
SA0252	lrgA	Holin-like protein LrgA	0.19
SA0253	lrgB	Holin-like protein LrgB	0.24
SA0276	—	Conserved hypothetical protein, similar to diarrheal toxin	0.51
SA0482	—	Hypothetical protein, similar to creatine kinase	0.54
SA0521	sdrE	Ser-Asp rich fibrinogen-binding, bone sialoprotein-binding protein	0.45
SA0650	norA	Quinolone resistance protein	0.53
SA0681	—	Hypothetical protein, similar to multidrug resistance protein	0.46
SA0835	clpB	ClpB chaperone homolog	0.43
SA0874	—	Hypothetical protein, similar to multidrug resistance protein-related protein	0.55
SA0900	sspB	Cysteine protease precursor	0.38
SA1000	—	Hypothetical protein, similar to fibrinogen-binding protein	0.41
SA1003	—	Hypothetical protein, similar to fibrinogen-binding protein	0.47
SA1004	—	Hypothetical protein, similar to fibrinogen-binding protein	0.53
SA1007	—	α-Hemolysin precursor	0.55
SA1617	—	Similar to latent nuclear antigen (Kaposi sarcoma-associated herpesvirus)	0.42
SA1660	cbf1	cmp-binding factor 1	0.52
SA1752	truncated(hlb)	Truncated β-hemolysin	0.47
SA1761	sep	Enterotoxin P (bacteriophage phiN315)	0.51
SA1812	—	Similar to synergohymenotropic toxin precursor, *Staphylococcus intermedius*	0.33
SA1813	—	Hypothetical protein, similar to leukocidin chain lukM precursor	0.35
SA1818	—	Hypothetical protein, similar to β-lactamase (pathogenicity island SaPIn1)	0.46
SA2431	isaB	Immunodominant antigen B	0.42
SA2447	—	Hypothetical protein, similar to streptococcal hemagglutinin protein	0.48
SA2457	—	Capsular polysaccharide biosynthesis, capA	0.55
Similar to unknown proteins (category V)			
SA0271	—	Conserved hypothetical protein	0.20
SA0275	—	Conserved hypothetical protein	0.40
SA0359	—	Conserved hypothetical protein	0.45
SA0360	—	Conserved hypothetical protein	0.44
SA0407	—	Conserved hypothetical protein	0.44
SA0637	—	Conserved hypothetical protein	0.54
SA0725	—	Conserved hypothetical protein	0.51
SA0739	—	Conserved hypothetical protein	0.53
SA0804	—	Conserved hypothetical protein	0.49
SA0856	—	Conserved hypothetical protein	0.43
SA0873	—	Conserved hypothetical protein	0.36
SA1016	—	Conserved hypothetical protein	0.50
SA1020	—	Conserved hypothetical protein	0.52
SA1021	—	Conserved hypothetical protein	0.51
SA1022	—	Conserved hypothetical protein	0.48
SA1030	—	Conserved hypothetical protein	0.54
SA1031	—	Conserved hypothetical protein	0.48
SA1062	—	Conserved hypothetical protein	0.43
SA1133	—	Conserved hypothetical protein	0.45
SA1136	—	Conserved hypothetical protein	0.50
SA1179	—	Conserved hypothetical protein	0.54

Table S3. Cont.

Gene information			
ORF	Name	Product	Ratio (Mu50Ω2/Mu50Ω1)
SA1618	—	Conserved hypothetical protein	0.43
SA2298	—	Conserved hypothetical protein	0.50
SA2474	—	Conserved hypothetical protein	0.48
SA2491	—	Conserved hypothetical protein	0.46
No similarity (category VI)			
SA0194	—	Hypothetical protein	0.46
SA0273	—	Hypothetical protein	0.32
SA0277	—	Hypothetical protein	0.49
SA0291	—	Hypothetical protein	0.40
SA0292	—	Hypothetical protein	0.47
SA0395	—	Hypothetical protein	0.41
SA0806	—	Hypothetical protein	0.50
SAS028	—	Hypothetical protein	0.49
SA0930	—	Hypothetical protein	0.54
SAS030	—	Hypothetical protein	0.48
SA1001	—	Hypothetical protein	0.36
SA1002	—	Hypothetical protein	0.30
SAS037	—	Hypothetical protein	0.48
SA1168	—	Hypothetical protein	0.44
SA1320	—	Hypothetical protein	0.50
SAS049	—	Hypothetical protein	0.53
SA1825	—	Hypothetical protein	0.40
SA2331	—	Hypothetical protein	0.30
SA2444	—	Hypothetical protein	0.47
SA2473	—	Hypothetical protein	0.38
SAV0411	—	Hypothetical protein	0.54
SAV0797	—	Hypothetical protein	0.51

ABC, ATP binding cassette; PTS, phosphotransferase system; IIBC, type B and C component of type II PTS.

Table S4. Phenotype microarray results of comparing Mu50Ω1 and Mu50Ω2

Mode of action	Substrate(s)
Phenotypes gained in Mu50Ω1 vs. Mu50Ω2	
C-source, alcohol	2-Aminoethanol
C-source, amide	Glucuronamide
C-source, amino acid	L-glutamic acid, L-aspartic acid, L-proline, L-asparagine, L-glutamine, Gly-Glu
C-source, carbohydrate	L-rhamnose; L-fucose; D,L-a-glycerol phosphate; D-melibiose; lactulose, adonitol, dulcitol, D-cellobiose; D-glucose-6-phosphate; D-fructose-6-phosphate; m-inositol; *N*-acetyl-D-mannosamine
C-source, carboxylic acid	Propionic acid, D-glucuronic acid, acetic acid, L-malic acid, D-galacturonic acid, succinic acid, fumaric acid, mono-methylsuccinate
C-source, fatty acid	Tween 20, Tween 40, Tween 80, L-ornithine
C-source, carbohydrate	D-tagatose, D-arabinose, palatinose, arbutin, D-fucose, 3-methylglucose, L-sorbose, gentiobiose, D-arabitol, *N*-acetyl-D-glucosaminitol, maltitol
C-source, carboxylic acid	Butyric acid, 2-oxovaleric acid, caproic acid, oxalomalic acid, *N*-acetyl-neuraminic acid
C-source, polymer	Pectin
P-source, organic	Phosphoryl choline, cysteamine-S-phosphate, D-glucosamine-6-phosphate, taurocholic acid, L-methionine sulfone
N-source, peptide	Arg-Gln, His-Gly, Cys-Gly, Gly-Leu, Gly-Phe, Gly-Gly
N-source, amino acid	L-glutamine
N-source, peptide	Tyr-Gln, Tyr-Glu
pH, deaminase	pH 9.5 + putrescine
Nucleic acid analog, purine	6-Mercaptopurine, 5-fluorouracil
Protein synthesis	Tylosin
Protein kinase C inhibitor	Chelerythrine
Toxic anion	Sodium cyanate, Sodium arsenate
Chelator, hydrophilic	EDTA
Nitro compound	2-Nitroimidazole
Ribonucleotide diphosphate (DP) reductase inhibitor	Hydroxyurea
Membrane, nonspecific binding	Protamine sulfate
Oxidizes sulfhydryls	1-Chloro-2,4-dinitrobenzene
Toxic anion	Sodium selenite
Tyrosine phosphatase inhibitor	Phenylarsine oxide
Oxidizing agent	D,L-thioctic acid
Respiration, uncoupler	Crystal violet
Phenotypes lost in Mu50Ω1 vs. Mu50Ω2	
Chelator, lipophilic	5,7-Dichloro-8-hydroxyquinoline
cAMP phosphodiesterase inhibitor	Caffeine
Membrane, detergent, cationic	Benzethonium chloride
Oxidizes sulfhydryls	Iodoacetate
Phenothiazine, anticholinergic	Trifluoperazine
Toxic anion, PO_4 analog	Sodium orthovanadate